



38 **Abstract**

39 The importance of carbon (C)-nutrient interactions to the prediction of future C uptake has long  
40 been recognized. The Energy Exascale Earth System Model (E3SM) land model (ELM) version 1  
41 is one of the few land surface models that include both N and P cycling and limitation (ELMv1-  
42 CNP). Here we provide a global scale evaluation of ELMv1-CNP using International Land Model  
43 Benchmarking (ILAMB) system. We show that ELMv1-CNP produces realistic estimates of  
44 present-day carbon pools and fluxes. Compared to simulations with optimal P availability,  
45 simulations with ELMv1-CNP produces better performance, particularly for simulated biomass,  
46 leaf area index (LAI), and global net C balance. We also show ELMv1-CNP simulated N and P  
47 cycling are in good agreement with data-driven estimates. We compared ELMv1-CNP simulated  
48 response to CO<sub>2</sub> enrichment with meta-analysis of observations from similar manipulation  
49 experiments. We show that ELMv1-CNP is able to capture the field observed responses for  
50 photosynthesis, growth, and LAI. We investigated the role of P limitation in the historical  
51 balance and show that global C sources and sinks are significantly affected by P limitation, as  
52 the historical CO<sub>2</sub> fertilization effect was reduced by 20% and C emission due to land use and  
53 land cover change was 11% lower when P limitation was considered. Our simulations suggest  
54 that introduction of P cycle dynamics and C-N-P coupling will likely have substantial  
55 consequences for projections of future C uptake.

56

57

58

59

60

61

62

63

64

65

66

67 Copyright statement:

68

69 *This manuscript has been authored by UT-Battelle, LLC under Contract No. DE-AC05-00OR22725 with the*  
70 *US Department of Energy. The United States Government retains and the publisher, by accepting the*  
71 *article for publication, acknowledges that the United States Government retains a non-exclusive, paid-*  
72 *up, irrevocable, world-wide license to publish or reproduce the published form of this manuscript, or*  
73 *allow others to do so, for United States Government purposes. The Department of Energy will provide*  
74 *public access to these results of federally sponsored research in accordance with the DOE Public Access*  
75 *Plan (<http://energy.gov/downloads/doe-public-access-plan>).*

76

77

78

79

80

81

82

83

84

85

86

87

88

89

90

91

92

93

94

95

96

97

98

99

## 100 1. Introduction

101 The recent global carbon (C) budget showed that over the last half century global  
102 fossil CO<sub>2</sub> emissions have increased from about 3 Pg C/yr in 1960s to about 9.5 PgC/yr in the  
103 last decade (Friedlingstein et al., 2019). It has also been shown that land ecosystems play  
104 important roles in controlling the fractions of CO<sub>2</sub> emissions that remain in the atmosphere  
105 by taking up about 29% of total emissions (Le Quéré et al., 2018). Large uncertainties  
106 remain on the net land-atmosphere C exchange, mainly due to difficulties in quantifying the  
107 complex C cycle processes such as CO<sub>2</sub> fertilization effects, responses of carbon fluxes to  
108 temperature and precipitation variation, and C emissions associated with land use and land  
109 cover change (LULCC). These uncertainties will very likely hamper our ability to predict the  
110 future trajectories of atmospheric CO<sub>2</sub>.

111 One of the important uncertainties relates to our understanding of C-nutrient  
112 interactions and nutrient limitation and how they are represented in models. The  
113 importance of nitrogen (N) availability to predicted land C storage has been long recognized  
114 (Hungate et al., 2003). Although there were only two models in CMIP5 (the fifth phase of  
115 the Coupled Model Intercomparison Project) that accounted for N dynamics and N  
116 limitation (Thornton et al., 2007; Thornton et al., 2009; Arora et al., 2013), many ESMs  
117 participating in CMIP6 (the Coupled Model Intercomparison Project phase 6) are now  
118 including N cycle and C-N interactions (Davies-Barnard et al., 2020; Lawrence et al., 2019;  
119 Goll et al., 2017a; Smith et al., 2014; Sellar et al., 2019). The comparisons between these  
120 models have been summarized in Arora et al. (2020) and Davies-Barnard et al. (2020). In  
121 recent years, significant efforts have also gone into understanding phosphorus (P) cycle  
122 dynamics and the role of P limitation in land C storage (Jiang et al., 2019; Hou et al., 2020;  
123 Reed et al., 2015; Wieder et al., 2015b; Sun et al., 2017). Increasing numbers of models  
124 have developed the capability to include P cycle processes and C-N-P interactions (Wang et  
125 al., 2010; Goll et al., 2012; Thum et al., 2019; Goll et al., 2017b; Yang et al., 2014; Yang et al.,  
126 2019; Sun et al., 2021). It has been shown that considering P cycle dynamics and C-N-P  
127 interactions improves process representation and model fidelity compared with  
128 observational and experimental data in most models (Goll et al., 2017b; Yang et al., 2014).

129 Model simulations have also demonstrated the importance of P limitation to land C uptake  
130 (Zhang et al., 2014; Goll et al., 2012; Yang et al., 2016; Yang et al., 2019; Sun et al., 2021).  
131 Using an ensemble of 14 terrestrial ecosystem models to simulate the planned free-air CO<sub>2</sub>  
132 enrichment experiment AmazonFACE, Fleischer et al. (2019) showed that P availability  
133 reduced the projected CO<sub>2</sub>-induced C sink by about 50% compared to estimates from  
134 models assuming no phosphorus limitation. Taken together, understanding and  
135 representation of the role of P cycle dynamics in affecting terrestrial C balance is essential  
136 for the prediction of future terrestrial carbon uptake and atmospheric CO<sub>2</sub> concentration.

137 Field and modeling studies have shown that forest productivity tends to increase with  
138 increasing soil phosphorus availability (Vicca et al., 2012; Aragão et al., 2009; Wang et al.,  
139 2010). Despite these recent efforts, P cycle dynamics and C-N-P interactions are not yet  
140 included in most CMIP6 models. The Energy Exascale Earth System Model(E3SM) is one of  
141 the few models that have been developed a coupled C-N-P capability in the land component  
142 in CMIP6 (Burrows et al., 2020). The land model in E3SM, herein referred to as ELMv1-CNP,  
143 has been first applied in the Amazon region to test its capability and to evaluate the  
144 importance of P limitation in this region (Yang et al., 2019). Yang et al. (2019) provides an in-  
145 depth evaluation of ELMv1-CNP for the Amazon rainforest using field observational data,  
146 with a focus on how the introduction of P cycle dynamics and P limitation improved model  
147 simulated spatial variation of productivity. They show that effects of P limitation on C  
148 sources and sinks in the Amazon region are significant, reducing simulated CO<sub>2</sub> fertilization  
149 of new carbon uptake by as much as 31%.

150 This study expands the analysis in the Amazon region to the global scale and has two  
151 main aims: (1) to provide an evaluation of ELMv1-CNP performance on the global scale  
152 using both observational and experimental data, and (2) to quantify the role of P cycle  
153 dynamics and P limitation in affecting simulated C sources and sinks globally. We first  
154 evaluate the performance of ELMv1-CNP using the ILAMB benchmarking system (Collier et  
155 al., 2018), which has been widely used in the evaluation of land surface models and ESMs  
156 (Lawrence et al., 2019; Bonan et al., 2019; Zhu et al., 2019; Friedlingstein et al., 2019). We  
157 then evaluate ELMv1-CNP simulated N and P pools and fluxes with an observation-based

158 dataset. Realizing that the static benchmarking may not help constrain future model  
159 projections, we further evaluate ELMv1-CNP using experimental manipulations of  
160 atmospheric CO<sub>2</sub>. Finally, we take advantage of the P-enabled capability in ELMv1-CNP to  
161 quantify the effect of P dynamics on the simulated ecosystem responses to increasing  
162 atmospheric CO<sub>2</sub>, increasing N deposition, LULCC, and climate change on the global scale.

163

## 164 **2. Method**

### 165 **2.1 Model Overview**

166 ELMv1-CNP is based on the Community Land Model version 4.5 (CLM4.5), which  
167 includes coupled C-N biogeochemistry from CLM4 (Thornton et al., 2007) and  
168 improvements to canopy photosynthesis, soil biogeochemistry and representation of  
169 nitrogen cycle dynamics (Koven et al., 2013; Bonan et al., 2011; Oleson et al., 2013).  
170 Recognizing the critical role of the tropical forests in the global carbon cycle and C-climate  
171 interactions and the important role of P cycle dynamics and P limitation in tropical forests,  
172 we implemented a fully prognostic P cycle and C-N-P interactions into ELMv1-CNP, enabling  
173 ELMv1-CNP to be one of the few land surface models that include both N and P cycle  
174 dynamics and limitation. The main model features include (1) a fully prognostic P cycle  
175 tracking various soil inorganic P pools, vegetation P pools, litter and soil organic P pools (2)  
176 the representation of P limitation on plant productivity and litter and soil organic matter  
177 decomposition based on a supply-demand approach (3) resolving N vs P limitation using  
178 the Liebig law (4) the vertically-resolved soil inorganic and organic P dynamics (5) the  
179 decoupling of P cycle from C and N cycle during decomposition due to phosphatase activity  
180 (6) the representation of adsorption-desorption dynamics based on soil order.

181 Besides the P cycling processes, the other important difference of ELMv1-CNP from  
182 CLM4.5 is the removal of instantaneous downregulation of photosynthesis from nutrient  
183 limitation. Instead, longer-term downregulation of productivity is enabled through the  
184 implementation of C, N, and P nonstructural vegetation storage pools. In CLM4.5, nutrient  
185 limitation is calculated at each time step as a function of potential GPP, stoichiometry of  
186 plant tissues, and nitrogen uptake. Any “excess” carbon due to nitrogen limitation is

187 immediately released to the atmosphere through instantaneous downregulation. This  
188 nutrient limitation can be highly variable over time and affects diurnal and seasonal cycles  
189 of gross primary productivity, which is not consistent with flux tower observations (Ghimire  
190 et al., 2016) or with short-term elevated CO<sub>2</sub> experiments that were done with and without  
191 nutrient fertilization (Metcalf et al., 2017). In the current model, competition for available  
192 nutrients and plant uptake still occur every timestep given instantaneous demand that is a  
193 function of plant GPP and microbial nutrient immobilization (Oleson et al.,  
194 2013). However, nutrients taken up by plants are now first allocated to non-structural N  
195 and P storage pools instead of directly to structural pools. Nutrient limitation to allocation  
196 is determined by comparing plant nutrient demand (given GPP and stoichiometry) and the  
197 nutrient availability from the non-structural nutrient pools, which is a function of the pool  
198 size in relation to long-term demand. The “excess” carbon flux, which cannot be allocated  
199 due to nutrient limitation, is directed to the non-structural plant carbon (NSC) pool instead  
200 of downregulating GPP. This pool respire to the atmosphere with a given turnover time.  
201 Details about the representation of NSC can be found in the supporting information (Text  
202 S1)

203 The model version used in this study is the publicly released ELM v1 and can be  
204 downloaded along with all the parameter files at <https://github.com/E3SM-Project/E3SM>.  
205 In this version of the model, the fire module is activated by default. The soil erosion module  
206 is not activated. We assume soil C, N, and P cycling can take place to the 3.8m depth as the  
207 assumption in CLM4.5 (Koven et al., 2013). We also provide the key model parameters in  
208 Table S1 (PFT specific) and Table S2 (soil order specific). We note that only leaf parameters  
209 vary with PFT, but we include all other tissues in Table S1 to provide all parameters in the  
210 consistent format.

211

## 212 **2.2 Simulations**

213 The simulations presented here were first spun up to bring C, N, and P pools to  
214 equilibrium by recycling the GSWP3 (Global Soil Wetness Project Phase 3) climate forcing  
215 data (<http://hydro.iis.u-tokyo.ac.jp/GSWP3/>) between 1901-1920, along with constant

216 atmospheric CO<sub>2</sub>, N deposition and land cover type at year 1850. Spinup was accomplished  
217 through two steps: accelerated decomposition (AD) spinup and regular spinup. We ran the  
218 model for 250 years in the AD spinup mode. The purpose of the AD spinup is to accelerate  
219 the decomposition process and speed up the spinup process of the carbon and nutrient  
220 cycles. The AD spinup procedure was modified from that originally described by Thornton  
221 and Rosenbloom (2005), which used spatially invariant acceleration factors to accelerate  
222 decomposition in soil organic matter (SOM) pools. Here we updated the AD spinup by  
223 including the impacts of temperature and soil moisture on the acceleration factor. This  
224 resulted in higher acceleration factors in cool and/or dry climates, which are typically slower  
225 to achieve steady state. In addition, vegetation dead stem and coarse root mortality  
226 were accelerated by a factor of 10 to achieve steady state biomass more quickly. The factor  
227 of 10 was chosen to have a good balance between faster acceleration and the  
228 disequilibrium between accelerated and non-accelerated steady states that requires a  
229 longer regular spinup following Koven et al. (2013). In the AD spinup, supplemental soil  
230 mineral P was applied for the entire simulation such that there was no P limitation on C and  
231 N dynamics. During the transition between AD spinup and regular spinup, we initialized the  
232 soil inorganic pools using global P maps developed by (Yang et al., 2013). For the grid cells  
233 that don't have values in Yang et al. (2013), we applied the nearest neighbor method to  
234 estimate the values. Since the P cycle involves both biological and geochemical processes  
235 that occur on geological time scales, the initialization of P pools provides some reasonable  
236 estimates of soil P pools without running the model for millions of simulated years. More  
237 details regarding the rationale of using the developed P maps for initialization can be found  
238 in Yang et al. (2013). We then ran normal spinup for 600 years with active C, N, and P  
239 coupled biogeochemistry until C, N, and P pools reached equilibrium. The criteria for  
240 equilibrium are for global total NEE less than 0.1 PgC/yr averaged over 100 years, the  
241 threshold recommended for the C4MIP (Jones et al., 2016). We also ran a control simulation  
242 between 1850-2010 as a continuation of the normal spinup. We added the time series of  
243 labile P, secondary mineral P and occluded P for the control simulation (Fig. S1). There are  
244 very little changes in the inorganic P pools during the 161 years control simulation



245 suggesting that these pools can be considered in equilibrium for the time scale of our  
246 interest.

247 After the model was spun up, we ran the global historical transient simulations (1850–  
248 2010) at 0.5 degree spatial resolution using GSWP3 v2 climate forcing data, along with  
249 historical transient atmospheric CO<sub>2</sub> concentration, N deposition, land use and land cover  
250 change that are part of the CMIP6 protocols (<https://luh.umd.edu/data.shtml>). Input data  
251 and references are summarized in Table S3. We also ran a suite of single-factor simulations  
252 to examine the individual effects of changing environmental factors (atmospheric CO<sub>2</sub>, land  
253 use and land cover change, climate, and nitrogen deposition, Table 1). In addition to the  
254 ELM v1 simulations with a fully active P cycle, we also performed historical transient and  
255 single-factor simulations with P limitation switched off (supplementing P availability to fully  
256 meet demand at each grid cell and for each timestep so there is no P limitation on  
257 productivity and decomposition). We denoted the default ELM v1 simulations that have an  
258 active P cycle as the CNP configuration (ELMv1-CNP) and simulations assuming no P  
259 limitation as the CN configuration (ELMv1-CN).

260 We also performed one additional simulation where we initiated a global step increase  
261 of atmospheric CO<sub>2</sub> concentration, by +200ppm, starting from 2001 and continuing through  
262 2010. These simulations are designed to mimic the Free Air CO<sub>2</sub> Enrichment (FACE)  
263 experiments (Ainsworth and Long, 2005). To quantify model sensitivities to elevated CO<sub>2</sub>,  
264 we calculated the effect size (treatment divided by control) over the 10 years of simulation  
265 (2001-2010). We then evaluated model sensitivities to elevated CO<sub>2</sub> against meta-analysis  
266 from FACE experiments (Ainsworth and Long 2005).

267 All of the simulations are summarized in Table 1.

268

### 269 **2.3. ILAMB**

270 We used the International Land Model Benchmarking system (Collier et al., 2018; Luo et  
271 al., 2012; Hoffman et al., 2017) to assess the model performance. ILAMB was designed to  
272 use a wide array of observational data to constrain model results, including various land  
273 carbon pools and fluxes, inferred CO<sub>2</sub> concentration variability, and functional relationships.

274 For each variable, ILAMB scores model performance for period mean, bias, root-mean-  
275 square error (RMSE), spatial distribution, interannual coefficient of variation, seasonal cycle,  
276 and long-term trend. These scores are aggregated into an overall score representing  
277 multiple aspects of model performance for each variable. These aggregated absolute scores  
278 are then used to calculate the relative score, which indicates the relative performance of  
279 each model with respect to other models used in the same analysis. The observational  
280 datasets used for the evaluation of carbon cycle in ILAMB are listed in Table S4.

281 In order to understand how the implementation of P cycling dynamics affects model  
282 performance, we evaluated the performance of both ELMv1-CNP and ELMv1-CN. In order to  
283 provide a context in terms of model performance in ILAMB, we provide the ILAMB  
284 evaluation of several other land models included in the Land Surface, Snow and Soil  
285 moisture Model Intercomparison Project (LS3MIP) as part of CMIP6 ([https://www.wcrp-  
286 climate.org/wgcm-cmip/wgcm-cmip6](https://www.wcrp-climate.org/wgcm-cmip/wgcm-cmip6)). LS3MIP includes a collection of model experiments  
287 including both offline land model experiments and coupled experiments (Van Den Hurk et  
288 al., 2016). We used the results from the offline land model experiments. Like our  
289 simulations, these experiments were performed at 0.5by0.5 spatial resolution and using the  
290 GSWP3 forcing data. Other model configurations in LS3MIP are identical to that used in  
291 CMIP6 historical simulations, which we used for the simulations in this study.

292

#### 293 2.4. GOLUM-CNP

294 Since there is no nutrient cycle metrics in ILAMB, we also compared major N and P pools  
295 and fluxes along with nutrient use efficiencies from ELMv1-CNP with the data-driven  
296 estimates of N and P pools and fluxes from the Global Observation-based Land-ecosystems  
297 Utilization Model of Carbon, Nitrogen, and Phosphorus (GOLUM-CNP) (Wang et al., 2018).  
298 GOLUM-CNP combines data-driven estimates of N and P inputs and outputs and observed  
299 stoichiometric ratios with a steady-state diagnostic model, providing global steady-state N  
300 and P pools and fluxes for large biomes. Despite large uncertainties and the steady-state  
301 assumptions, GOLUM-CNP provides a global data-driven product that can be used to test

302 nutrient cycles in land surface models. GOLUM-CNP has also been used in the evaluation of  
303 other land surface models (Sun et al., 2021).

304

### 305 **3. Results**

#### 306 **3.1 Evaluations of ELM v1 using ILAMB**

307 ILAMB includes many metrics that cover water, energy, and carbon pools and fluxes on  
308 both regional and global scales. Fig. 1 shows ILAMB benchmarking scores for ELMv1-CNP  
309 and ELMv1-CN, along with several other land models in CMIP6, which are provided to  
310 contextualize ILAMB scores for ELMv1-CNP. The relative model performance scores are  
311 shown in Fig. 1, indicating which model version performs better with respect to others. The  
312 full results produced by the ILAMB package can be found at [https://compy-  
313 dtn.pnl.gov/yang954/build/](https://compy-dtn.pnl.gov/yang954/build/).

314 Fig. 1 shows that the performance of ELMv1-CNP is comparable to other land models in  
315 CMIP6. ELMv1-CNP exhibits performance similar to CLM5 (CESM2) in terms of aggregated  
316 scores for carbon cycle metrics, while CLM5 shows better performance with respect to  
317 overall functional relationships, mainly due to a better score for functional relationship of  
318 burned area. The performance of each model varies for different variables. For example,  
319 ORCHIDEE land surface model in IPSL-CM6A-LR performs relatively well in inferred  
320 atmospheric carbon dioxide, leaf area index and GPP relationships.

321 Fig.1 also shows the comparison between ELM v1-CNP and ELM v1-CN, allowing us to  
322 quantify the impacts of including a prognostic P cycle and realistic P availability on model  
323 performance. For metrics in Fig. 1 that show the greatest differences between ELMv1-CNP  
324 and ELMv1-CN, the CNP version always has a higher score than CN. This is reflected in the  
325 relatively higher aggregated scores for carbon cycle variables and functional relationships  
326 in ELMv1 -CNP.

327

328 Fig. 2 shows the Global Net Ecosystem Carbon Balance metric in ILAMB for ELM v1-CNP  
329 and ELM v1-CN. The observational data sets for this metric are from the Global Carbon  
330 Project (Fig. 2a)(Le Quéré et al., 2016) and from the inversion-based estimate (Hoffman et

331 al., 2014), both providing global totals of land carbon accumulation but for different  
332 historical time period (1850-2010 for Hoffman et al., 2014 and 1959-2010 for Le Quere et l.,  
333 2016). The simulated global C balance by both ELMv1-CNP and ELMv1-CN are in the range  
334 of uncertainty of observational estimates, with ELMv1-CNP simulated historical global  
335 carbon accumulation being a better match with mean observational estimates, particularly  
336 after 1950. ELMv1-CN estimated a net accumulation of land carbon of 22 Pg C over the  
337 period 1850-2010, which is much higher than the mean observational estimate of - 8Pg C.  
338 ELMv1-CNP estimated land carbon accumulation of 7 Pg C.

339 Fig. 3 shows the spatial distribution of vegetation biomass for the benchmark data and  
340 model bias in ILAMB. Overall both ELMv1-CN and ELMv1-CNP tend to overestimate  
341 biomass, compared to this specific global product of biomass (GEOCARBON). The high bias  
342 in the tropical region is much reduced in ELMv1-CNP simulations (Fig. 3a, 3b and 3c). The  
343 better performance of ELMv1-CNP is also reflected in the spatial Taylor diagram for  
344 biomass (Fig. 3d).

345 Another important benchmark in ILAMB is the functional relationships between two  
346 variables, for example the relationship between GPP and precipitation and the relationship  
347 between annual mean LAI and precipitation. An accurate simulation of these relationships  
348 in addition to individual benchmarks is an indication that the models are representing the  
349 underlying processes correctly. ELMv1-CNP produces a better functional relationship  
350 compared to ELMv1-CN. For example, for the relationship between LAI and precipitation  
351 ELMv1-CN overestimated LAI, particularly in regions with high precipitation, while the  
352 ELMv1-CNP configuration shows an improved relationship (Fig. 4). The improvement of the  
353 functional relationship is mainly due to the improvement in high precipitation regions, e.g.  
354 lowland tropical forest regions. In these regions, inclusion of P dynamics and P limitation  
355 reduced simulated bias in GPP and LAI, therefore leading to better match with the  
356 observations.

357

358 3.2. Evaluation of N and P cycling in ELMv1-CNP

359 We evaluated simulated nutrient use efficiencies against that from GOLUM-CNP product  
360 on the biome level. Here we define nutrient use efficiency as the ratio between annual NPP  
361 and annual nutrient uptake (for both N and P), with NUE for nitrogen use efficiency and  
362 PUE for phosphorus use efficiency (Finzi et al., 2007). ELMv1-CNP simulated NUE is higher  
363 in temperate and boreal forests and lower in tropical grassland and tundra, which is  
364 consistent with GOLUM-CNP (Fig. 5a). [Temperate grassland NUE and PUE in ELMv1-CNP are  
365 higher in distribution because of the higher variation in NPP allocation to non-structural  
366 carbon pools.](#) ELMv1-CNP predicted higher NUE in tropical lowland forests than GOLUM-  
367 CNP. ELMv1-CNP simulated PUE is generally consistent with GOLUM -CNP (Fig. 5b).  
368 However, ELMv1-CNP simulated PUE in tropical forests is much lower than that from  
369 GOLUM-CNP.

370 We also evaluated ELMv1-CNP simulated N and P pools and major fluxes on the global  
371 scale for the period of 2001-2010 with the observationally derived products in GOLUM-  
372 CNP. Fig. S2 shows the comparison of N and P uptake from ELMv1-CNP and GOLUM-CNP at  
373 the biome level. ELMv1-CNP simulated plant N and P uptake is in agreement with GOLUM-  
374 CNP, with higher uptake fluxes in tropical forests and lower uptake in temperate and boreal  
375 forests. ELMv1-CNP simulated N uptake is lower in the tropical forests, compared to  
376 GOLUM-CNP (Fig. S2a). Conversely, simulated P uptake is higher than GOLUM-CNP  
377 estimates across the tropics (Fig. S2b).

378

### 379 **3.2 Evaluations using CO<sub>2</sub> manipulation experiment**

380 Relative to the control simulation, increasing atmospheric CO<sub>2</sub> concentration by 200ppm  
381 increased gross primary productivity by 23% (global mean) over the 10 years of simulation  
382 (2001-2010). Nearly all PFTs showed more than a 10% increase in productivity, with more  
383 significant increases occurring in tropical regions and middle latitudes (Fig. 6a). The  
384 modeled response ratio of NPP is also showing widespread increases, and on the global  
385 scale our results showed a 25.8% increase in NPP in response to CO<sub>2</sub> enrichment (Fig. 6b).  
386 The simulated increases in GPP and NPP also showed, to a large extent, translated into  
387 increases in vegetation carbon (Fig 6c), with a global average response ratio of 18%. The

388 modeled response ratio of LAI is much smaller, a 5% increase globally (Fig 6d). The globally  
389 aggregated simulated effect size of CO<sub>2</sub> enrichment from ELMv1-CNP on GPP, NPP, LAI and  
390 NSC compare well to the observations from the meta-analysis (Fig. 7), particularly for GPP  
391 and LAI. ELMv1-CNP overestimated the responses of NPP. Both observations and  
392 simulations show large sensitivity of NSC to CO<sub>2</sub> enrichment, with larger variability in the  
393 model simulations.

394

### 395 **3.3. Carbon, nitrogen and phosphorus pools and fluxes**

#### 396 **3.3.1 Carbon budget**

397 Major components of the global land C budget for present day (mean of 2001–2010) in  
398 ELMv1-CNP are shown in Fig 8a. These are from historical simulations with transient climate  
399 forcing, atmospheric CO<sub>2</sub> concentration, land use and land cover change, and N deposition.  
400 For the present day, model simulated total ecosystem C is 2588.73 Pg C, with about 22%  
401 stored in vegetation (575.45 Pg C), about 5% stored in litter and coarse wood debris (122.5  
402 Pg C), and 73% stored in soil organic matter (1890.78 Pg C). Model simulated vegetation C is  
403 within the range of inventory-based estimates from IPCC AR5 (450–650 Pg C). Our simulated  
404 vegetation C is also comparable to or slightly higher than observational estimates from the  
405 literature: 455Pg C (GEOCARBON, (Avitabile et al., 2016; Santoro et al., 2015), 550±100 Pg C  
406 (Houghton, 2003), 560±94 Pg C (Defries et al., 1999), and 450 Pg C (Erb et al., 2018). Model  
407 simulated total soil C is within the range of estimates from IPCC AR5 (1500-2400 Pg C) and  
408 that from Jobbágy and Jackson (2000) (1750±250 PgC). Model simulated total soil C is lower  
409 than several other observational estimates from the literature: 2376-2456 (Batjes, 2014),  
410 3000 Pg C (Köchy et al., 2015), which could be because ELMv1-CNP has yet to include an  
411 explicit representation of peatland carbon dynamics. As for the top 1m soil carbon, model  
412 simulated values of 1134.41 Pg C are within the range of estimates from the Harmonized  
413 World Soil Database (HWSD) (FAO/IIASA/ISRIC/ISSCAS/JRC, 2012) as reported by Todd-  
414 Brown et al. (2013) (890-1660 Pg C), but lower than the observational based estimate of  
415 1462–1548 Pg C from Batjes (2014) and 1325 Pg C from Köchy et al. (2015). Model  
416 simulated litter C (22.9 Pg C) is lower than the observational based estimate: 68 Pg C

417 (Matthews, 1997) and  $43 \pm 3$  Pg C (Pan et al., 2011). Model simulated coarse wood debris C  
418 stock (99.6 Pg C) is higher than the observational based estimate: 75 Pg C (Matthews, 1997)  
419 and  $73 \pm 6$  Pg C (Pan et al., 2011).

420 Model simulated present day GPP(134.15 Pg C/yr) is slightly higher than observational  
421 based estimate:  $123 \pm 8$  Pg C/yr (Beer et al., 2010),  $119 \pm 6$  Pg C/yr (Jung et al., 2011) and 123  
422 PgC/yr (IPCC AR5), and lower than 150-175 Pg C/yr from Welp et al. (2011) that is derived  
423 based on oxygen isotopes of atmospheric CO<sub>2</sub>. A recent study based on satellite data  
424 suggested a global GPP of 140 Pg C/yr for year 2007 (Joiner et al., 2018). The comparisons  
425 between simulated carbon pools and fluxes and available observations are also included in  
426 Table 2.

427

### 428 **3.3.2. Nitrogen budget**

429 The ELMv1-CNP estimated N budget for the present day (2001–2010) is summarized in  
430 Fig 8b. Compared to the C cycle, there are fewer observational estimates for N pools and  
431 fluxes. Most of the literature values are from other model simulations. Although not  
432 appropriate for direct model evaluation, these modeling estimates from the literature  
433 provide a broad context for us to evaluate our simulated pools and fluxes.

434 Model simulated vegetation N is 4.36 Pg N, which is comparable to the estimates from  
435 some other modeling studies: 3.8 Pg N (Zaehle et al., 2010), 5.3 Pg N (Xu and Prentice,  
436 2008) and lower than the estimates of 16 Pg N(Lin et al., 2000) and 18 Pg N (Yang et al.,  
437 2009). Model simulated total soil organic matter N is 188.79 Pg N, which is reasonable  
438 considering the observational based estimate for 1m of 95 Pg N (Post et al., 1985) and 133–  
439 140 Pg N (Batjes, 2014). ELMv1-CNP estimated biological nitrogen fixation (BNF) of 89  
440 TgN/yr is within the range of estimates from literature. Vitousek et al. (2013) estimated that  
441 global BNF ranges between 40–100 TgN/yr using a mass-balance approach. A meta-analysis  
442 by Davies-Barnard and Friedlingstein (2020) suggested that global inputs of BNF in natural  
443 ecosystems range between 52 and 130 TgN/yr, with a median global value of 88 TgN/yr. For  
444 the purpose of comparison, BNF estimates from CLM5 is 96.4 TgN/yr, slightly higher than

445 our estimate. The comparisons between simulated N pools and fluxes and available  
446 observations are also included in Table 2.

447

448

### 449 **3.3.3 Phosphorus budget**

450

451 The ELMv1-CNP estimated P budget for the present day (2001–2010) is summarized in  
452 Fig 8c. Very few observational data are available for P on the global scale. The only  
453 observation-based global product is the global P maps developed by (Yang et al., 2013).  
454 Model simulated vegetation P is 0.36 Pg P, which is comparable to the estimates from other  
455 modeling studies ranging from 0.23 to 3 Pg P (Goll et al., 2012; Wang et al., 2010; Jahnke,  
456 1992). Model simulated soil organic P is 3.75 Pg P, which is slightly lower than previous  
457 studies 5.74 Pg P (Goll et al., 2012), 5-10 Pg P (Smil, 2000), and 8.6 Pg (Yang et al., 2013).  
458 Model simulated soil mineral P for the top 40cm and 60cm is 63.24 Pg P and 81.32 Pg P  
459 respectively, which are generally comparable to the estimate of 45 Pg P for top 50cm soil  
460 from Yang et al. (2013). The comparisons between simulated P pools and fluxes and  
461 available observations are also included in Table 2.

462

### 463 **3.4. The effects of P limitation on historical carbon cycle**

464 ELMv1-CNP calculates the extent of both N and P limitation for plant growth on the  
465 global scale (Figs. 9a and 9b). Generally speaking, P is a more limiting nutrient in tropical  
466 evergreen forests and savannas in South America and Africa, while N is more limiting in  
467 temperate regions (Fig. 9a). The ratio between the P limitation factor and N limitation  
468 factor illustrates the degree of N-P colimitation (Fig. 9b). N and P are co-limiting  
469 productivity in tundra, boreal forests, and deserts.

470 Fig. 10 shows the simulated spatial patterns of productivity and carbon storage and  
471 how they are affected by P dynamics and limitation. P dynamics strongly control land  
472 carbon uptake and storage, particularly in tropical regions. Globally NPP is highest in  
473 tropical evergreen forests and lower in middle to high latitude regions. Plant growth in  
474 tropical regions, however, is generally limited by P availability, particularly in the central



475 and eastern Amazon basin and tropical Africa. The reduced productivity due to P limitation  
476 translates into reduced vegetation carbon storage and soil carbon storage, with the  
477 exception of tropical savannas, where fire dynamics also play an important role in  
478 vegetation and soil carbon storage.

479  
480 Fig. 11 shows the effects of P dynamics on historical global land carbon  
481 accumulation. The introduction of P dynamics leads to a 19.5% reduction in global C  
482 storage due to CO<sub>2</sub> fertilization between 1850 and 2010. The consideration of P dynamics  
483 also leads to a lower estimate of land use emissions on the global scale(143.89 PgC vs  
484 161.21 PgC) as CNP simulations generally show lower initial vegetation biomass. Increasing  
485 N deposition generally leads to a small carbon accumulation between 1850 and 2010 in  
486 both CN and CNP simulations globally. With P limitation, however, the global carbon  
487 accumulation from N deposition is reduced by about a third. Climate, although responsible  
488 for the large seasonal and interannual variability of carbon fluxes, has only minor impacts  
489 on historical carbon accumulation on the global scale for both CN and CNP simulations.  
490 When changes of all environmental factors are considered, the impact of P dynamics on  
491 carbon accumulation is the balance between a smaller CO<sub>2</sub> fertilization effect and lower  
492 land use emissions, with the net effect being slightly lower historical carbon accumulation  
493 globally.

494

## 495 **4. Discussions**

### 496 **4.1. ILAMB benchmarking**

497 This study presents a global assessment of the ELMv1-CNP. Yang et al. (2019) evaluated  
498 the performance of ELMv1-CNP in the Amazon region using plot-level observations from the  
499 RAINFOR network and found that the model captures well the observed productivity and  
500 biomass gradient across the Amazon basin. Here we further evaluate the global model  
501 performance using the ILAMB benchmarking system – an open source land model  
502 evaluation system that is designed to assess model performance at site level, regional, and  
503 global scales in an integrated and comprehensive way.

504 We include several other land models in CMIP6 in our ILAMB analysis with the goal of  
505 providing a context for the performance of ELMv1-CNP. We found that ELMv1-CNP exhibits  
506 similar performance to other models. It is challenging to demonstrate a clear improvement  
507 or degradation for complex land surface models in ILAMB. For example, our analysis  
508 indicates that ELMv1-CNP performance is comparable to CLM5 in terms of the overall  
509 carbon cycle. Both ELMv1-CNP and CLM5 have a common ancestor CLM4.5, but they took  
510 very different approaches for further development. CLM5 had significant efforts undertaken  
511 in improving the representation of nitrogen cycle, while ELMv1-CNP was more focused on  
512 implementing a prognostic phosphorus cycle and C-N-P interactions. Model development  
513 activities in both models helped improved model performance through the lens of ILAMB  
514 but the sources of improvements are quite different. This highlights the need to include  
515 more process-level evaluations in ILAMB for the purpose of evaluating the impact of specific  
516 model improvements.

517 Although CLM5 and ELM-CNP perform similarly in terms of ILAMB scores, it is worth  
518 noting the unique role of P cycle dynamics in affecting C cycling and the importance of  
519 including P cycle limitation in earth system models for better prediction of carbon-climate  
520 feedbacks. The important role of soil P availability in affecting plant growth in tropical  
521 forests residing on highly weathered soils has long been recognized (Walker and Syers,  
522 1976; Vitousek et al., 2010; Butler et al., 2018; Elser et al., 2007). Recent work has also  
523 explored how increasing demand for P may attenuate predicted increase in NPP  
524 conceptually by comparing potential demand with potential nutrient available in the 21<sup>st</sup>  
525 Century (Wieder et al., 2015b; Sun et al., 2017). Increasing numbers of land models have  
526 incorporated P cycle dynamics and P limitations (Sun et al., 2021; Nakhavali et al., 2021).  
527 Although both N and P limitation acts through reducing NPP, it is critical to include P cycling  
528 explicitly in models since P cycle dynamics are very different from the N cycling dynamics.  
529 The primary input for P is through rock weathering, which make it a very much non-  
530 renewable nutrient for the terrestrial ecosystems, whereas N fixation, the primary input for  
531 N, is more biologically driven. P cycling involves the transformation of various forms of P  
532 through a series of biological, enzymatical and geochemical processes with the turnover

533 time ranging from seconds to millions of years. N cycle dynamics are relatively simpler, with  
534 two inorganic forms and mostly biological and enzymatical processes involved. In addition,  
535 the interactions between N and P cycling also points to the need to include P cycle explicitly  
536 in land models. Increasing numbers of studies have shown that biological N fixation could  
537 be constrained by soil P availability (Hungate et al., 2004; Reed et al., 2013; Barron et al.,  
538 2008; Edwards et al., 2006; Crews et al., 2000). On the other hand, studies have also shown  
539 that increases in N availability can promote phosphatase activity and enhance biochemical  
540 mineralization and therefore accelerate P cycling (Mcgill and Cole, 1981; Wang et al., 2007;  
541 Houlton et al., 2008; Olander and Vitousek, 2000; Treseder and Vitousek, 2001; Marklein  
542 and Houlton, 2012). We will continue refine and improve the representation of the C-N-P  
543 interactions in the future development of ELM.

544 Also, ILAMB, despite being a comprehensive benchmarking tool for land surface models,  
545 is limited in scope in terms of the benchmarking data included. For example, Quesada et al.  
546 (2012) found that the decreasing west-east gradient in productivity is mostly related to total  
547 soil P across the Amazon basin. Yang et al. (2019) showed that consideration of soil P  
548 availability improved model simulated productivity, enabling the model to capture the  
549 productivity gradient from west to east across the Amazon basin. The problem is that this  
550 productivity gradient across the Amazon basin is not captured in ILAMB benchmark data so  
551 the “failure” of a CN model would not be captured by ILAMB.

552 We show that the model performance generally improved with realistic P availability  
553 through the implementation of a prognostic P cycle in ELM. Compared to ELMv1-CN,  
554 ELMv1-CNP simulated biomass has lower bias across the tropical regions as P limitation  
555 leads to lower productivity and hence lower biomass. ELMv1-CNP produces better ILAMB  
556 scores on the functional relationships between GPP, LAI and other forcing variables, mainly  
557 due to improved estimates of GPP and LAI in tropical regions. ELMv1-CNP also produces  
558 higher ILAMB scores for the integrated benchmarks such as global net ecosystem carbon  
559 balance and carbon dioxide concentration. We note that satisfactory performance for these  
560 two integrated metrics is most critical to a land model in ESMs as they are most relevant to  
561 the coupling between land ecosystems and radiatively-forced climate change.

562 ELMv1-CNP is not always better than ELMv1-CN from the benchmarks in the current  
563 ILAMB system. One of the benefits of a multi-metric analysis package like ILAMB is that we  
564 can compare performance at different levels of granularity, and it is rare that any one  
565 model has uniformly improved performance over any other single model on every fine-  
566 grained metric. By having multiple data sources for a given metric we can often see  
567 improvement against one data source and degradation compared to another for the same  
568 model output. For example, the ELMv1-CN model performs better than ELMv1-CNP for  
569 ecosystem respiration when comparing the Fluxnet metric, but ELMv1-CNP does better  
570 than ELMv1-CN for the GBAF metric on the same output variable. In the case of GPP and  
571 NEE, although ELMv1-CN is performing better or the same as ELMv1-CNP for both Fluxnet  
572 and GBAF metrics, the overall better scores of the ELMv1-CNP model for the relationship  
573 metrics connected to GPP give us more confidence that ELMv1-CNP is actually an  
574 improvement. Each metric has its own advantages and disadvantages, and there is still  
575 considerable subjectivity in how to interpret the multi-metric collection. For example, the  
576 site-level evaluations in ILAMB do not take into account site-specific disturbance histories,  
577 which can be an important driver of NEE variability over time at a given site.

578  
579 Although the ILAMB benchmarking system is very useful for evaluating model  
580 performance from different aspects simultaneously, interpretation of ILAMB scores  
581 deserves extra caution with known observational bias considered. For example, ILAMB uses  
582 LAI estimated from remote sensing observations from the Moderate Resolution Imaging  
583 Spectroradiometer (MODIS) as benchmarking data, while studies have suggested that  
584 MODIS LAI may be biased low due to reflectance saturation in dense canopies in the  
585 tropical forests (Shabanov et al., 2005; Huete et al., 2002; Kobayashi and Dye, 2005).  
586 Another example is the observational data for biomass. There are significant differences  
587 between the “tropical” and “GlobalCarbon” datasets and the “GeoCarbon” dataset for  
588 tropical biomass, but they were given about the same default weight in the ILAMB scoring  
589 system. Mitchard et al. (2014) investigated the marked differences between different  
590 estimates of Amazon biomass and suggested the regional biases in some remote sensing

591 products might be due to the lack of consideration of ecological variation in tree wood  
592 density and allometry. Further investigation of these datasets is needed to ensure the  
593 quality of biomass benchmarking data.

594  
595 The current version of ILAMB includes analysis of 28 variables using more than 60  
596 datasets or data products. None of these variables, however, are directly related to nutrient  
597 cycles. As more land surface models are implementing N and P dynamics, it is becoming  
598 increasingly important to include metrics for nutrient stocks and fluxes. Davies-Barnard et  
599 al. (2020) assessed five nitrogen-enabled land surface models in CMIP6 and called out the  
600 need to have better constraints of nitrogen cycle processes. The need is equally urgent, if  
601 not more, to synthesize more observations to better constrain the P cycle processes, as less  
602 synthesized data are available for P. Encouragingly, recent studies have started to develop  
603 observational datasets based estimate of N and P cycling on the global scale for model  
604 evaluation, such as the GOLUM-CNP dataset we used in this study. We hope to highlight the  
605 need and engage the broader community in developing additional nutrient datasets that  
606 can be included in ILAMB.

607 Other metrics that would be useful are the responses from N and P addition  
608 experiments. As Yang et al. (2014) showed, fertilization experiments at sites along the  
609 Hawaii chronosequence provided a useful evaluation testbed to assess model simulated  
610 responses to N and P fertilization effects. FACE experiments are useful for model evaluation  
611 as shown here (section 4.2) and in other studies (Wieder et al., 2019; Davies-Barnard et al.,  
612 2020). Warming studies that include an explicit focus on nutrient cycle responses will be  
613 another good evaluation opportunity (Melillo et al., 2002). An existing challenge is to  
614 provide a common protocol to use these types of experiments in the ILAMB benchmarking  
615 system.

616

#### 617 4.2 Evaluations using GOLUM-CNP

618

619 On the biome level ELMv1-CNP simulated nutrient use efficiencies are consistent with  
620 the observation-based estimates from GOLUM-CNP. This indicates that the representation

621 of N and P cycling and C-N-P coupling is reasonable in ELMv1-CNP. In terms of nutrient  
622 uptake, both show the highest N and P uptake in tropical forests, due to the high N and P  
623 demand associated with high productivity. ELMv1-CNP predicted lower N uptake in the  
624 tropical forests, compared to GOLUM-CNP. Nutrient uptake in ELMv1-CNP is a function of  
625 nutrient availability and nutrient demand, with demand being determined by available  
626 carbon for allocation, allocation fractions to different plant tissues and plant tissue  
627 stoichiometry. The simulated NPP at the biome level matches well with NPP from GOLUM-  
628 CNP except for Tundra (Fig. S3). The different C:N and C:P stoichiometric ratios for  
629 vegetation tissues used in ELMv1-CNP and GOLUM-CNP could also contribute to the  
630 difference in . C:N ratios of leaf, wood, and fine root in GOLUM-CNP are all lower than  
631 ELMv1-CNP (21, 126, and 40 in GOLUM vs 30, 500, and 42 in ELMv1-CNP). This suggests for  
632 given amount of carbon allocation, N uptake would be lower in ELMv1-CNP. Soil P  
633 availability might be overestimated considering ELMv1-CNP estimated P leaching is much  
634 lower than the estimate of Wang et al. (2018), therefore leading to relatively higher P  
635 uptake in ELMv1-CNP. Differences in allocation factors could also be contributing to the  
636 differences in nutrient uptake between ELMv1-CNP and GOLUM-CNP. For example, the  
637 mean allocation fraction to fine root is higher in GOLUM-CNP compared to ELM-CNP, while  
638 allocation fraction to leaf is lower in GOLUM-CNP, particularly in forest ecosystems (Fig. S4  
639 and S6). GOLUM-CNP also has higher NPP allocation fraction to woody biomass in boreal  
640 forests (Fig. S5)

641

### 642 **4.3. Evaluations using CO<sub>2</sub> manipulation experiments**

643 Our simulated large increase in GPP with CO<sub>2</sub> enrichment (23%) is in agreement with  
644 field observations that photosynthetic assimilation increased 28% under elevated CO<sub>2</sub>  
645 (Ainsworth and Long, 2005). Our simulated 26% increase in NPP is higher than the 17%  
646 increase in observed increase in dry matter production in the FACE experiments (Ainsworth  
647 and Long, 2005; Wieder et al., 2019). Our simulated 18% increase in biomass is higher than  
648 the estimates from Terrer et al. (2019), which provides a data-driven estimate of global CO<sub>2</sub>  
649 fertilization effect on biomass and show a relative increase in biomass of 12±3% for a 250

650 ppm CO<sub>2</sub> increase. A meta-analysis of woody plants responses to elevated CO<sub>2</sub> shows a  
651 mean effects of 22.3% on biomass (Baig et al., 2015). Among CLM4, CLM4.5 and CLM5,  
652 ELMv1-CNP is more comparable to CLM5 with a strong simulated response of GPP, NPP, and  
653 vegetation carbon in response to CO<sub>2</sub> enrichment, while CLM4 and CLM4.5 showed very  
654 weak CO<sub>2</sub> effects (Wieder et al., 2019).

655 The much stronger sensitivity of photosynthesis to elevated CO<sub>2</sub> in ELMv1-CNP is due to  
656 the removal of instantaneous downregulation of photosynthesis as a response to nutrient  
657 limitation. The instantaneous downregulation assumption in CLM4 and CLM4.5 has been  
658 shown to be inconsistent with experimental results (Metcalf et al., 2017). Despite large  
659 uncertainty, it is encouraging that simulated NSC response to elevated CO<sub>2</sub> is largely  
660 consistent with the observational data (Fig. 7). The low sensitivity of LAI in ELMv1-CNP is  
661 also consistent with field observations. Our results suggest the assumption we made  
662 regarding the fate of photosynthate is reasonable. Yang et al. (2016) showed that enhanced  
663 phosphatase enzyme production response to increasing CO<sub>2</sub> could have important impacts  
664 on P availability and sustain forest productivity under elevated CO<sub>2</sub>. In simulating the  
665 planned free-air CO<sub>2</sub> enrichment experiment AmazonFACE, ELMv1-CNP simulated  
666 phosphatase activity increased about 20% over 15 years (Fleischer et al., 2019). Here we  
667 show that introduction of NSC pools further improve the response of vegetation processes  
668 to changes in P availability and P limitation.

669  
670 Our findings are consistent with field studies that show the strong increase of NSC under  
671 elevated CO<sub>2</sub> condition (eCO<sub>2</sub>), particularly when nutrient availability is low (Wong, 1990;  
672 Körner et al. (2005). Several studies evaluating CLM4.5 using carbon isotope data also  
673 suggested that model performance would be better with the introduction of an NSC pool  
674 (Mao et al., 2016; Raczka et al., 2016; Duarte et al., 2017). However, large uncertainties  
675 remain regarding the turnover rate of the NSC pool. Further synthesis of field  
676 measurements on NSC in CO<sub>2</sub> enrichment experiments are needed to evaluate and  
677 constrain the representation of NSC in models.

678 Our simulated strong sensitivity of photosynthesis to CO<sub>2</sub> enrichment is consistent with  
679 recent studies that show large GPP growth during the twentieth century (Campbell et al.,  
680 2017; Haverd et al., 2020; Ehlers et al., 2015). Ellsworth et al (2017) also showed a large  
681 increase of photosynthesis in response to elevated CO<sub>2</sub> in a temperate forest FACE  
682 experiment.

683 The increased sensitivity of GPP and NPP to CO<sub>2</sub> enrichment in ELMv1-CNP, compared  
684 with the predecessors CLM 4 and CLM4.5, will very likely reduce the bias in the atmospheric  
685 fraction of human CO<sub>2</sub> emissions in previous coupled simulations as noted by Hoffman et al.  
686 (2014). In fact, CO<sub>2</sub> concentration metrics in ILAMB, which translate model simulated NEE  
687 into atmospheric CO<sub>2</sub> signal using an atmospheric transport model (Collier et al., 2018), is  
688 intended for the evaluation of this sensitivity. The inferred atmospheric CO<sub>2</sub> concentration  
689 from ELM v1 is very reasonable compared with observed NOAA flask data (Fig. S7 and S8).

690

#### 691 **4.4. Model estimated carbon, nitrogen, and phosphorus pools and fluxes**

692 Global C, N, and P pools in our ELMv1-CNP simulation are in good agreement with  
693 recent independent global estimates, indicating that ELMv1-CNP is capable of simulating  
694 the contemporary C, N and P cycles. In Yang et al. (2019) it was shown that introduction of  
695 more realistic mortality processes improved the model representation of longitudinal  
696 spatial patterns of biomass across the Amazon basin. Here we show that an overall high  
697 bias in biomass production is corrected through limits of vegetation production in response  
698 to P availability, without compromising the improved spatial gradients obtained through  
699 the mortality mechanism. It is worth mentioning that our understanding of nutrient stocks  
700 and fluxes is much less advanced in comparison with the global C cycle. This has been  
701 increasingly acknowledged for the global N cycle as increasing numbers of land surface  
702 models have incorporated N cycle dynamics and C-N interactions (Zaehle et al., 2010;  
703 Wieder et al., 2019; Davies-Barnard et al., 2020; Smith et al., 2014; Sellar et al., 2019; Goll  
704 et al., 2017a; Gerber et al., 2010). Biological N fixation and N-use efficiency have been  
705 identified as the key processes that need to be better constrained for land surface models  
706 (Davies-Barnard et al., 2020).



707 Our understanding of P stocks and fluxes are even less advanced than that for the N  
708 cycle, as shown in this study and other modeling studies that include P as a limiting  
709 nutrient. This is mainly due to: (1) various forms of P with different level of availability for  
710 plants and microbes, (2) geochemical processes in conjunction with biological processes  
711 controlling P availability, and (3) technical challenges in measuring soil P. For example,  
712 Hedley fractionation data provide a comprehensive picture of different P forms in soils and  
713 has been used for model evaluation and/or initialization in all the land surface models that  
714 include a prognostic phosphorus cycle (Wang et al., 2010; Goll et al., 2012; Yang et al.,  
715 2014; Yang et al., 2019). However, this extraction method is time-consuming and  
716 challenging, and not many routine measurements have been made using this technique.  
717 As such, observational estimates of P pools and fluxes are extremely limited. Although  
718 recent global Hedley database development (Yang and Post, 2011; Hou et al., 2018) has  
719 been helpful in global model development and evaluation, more observational data on P  
720 stocks and fluxes are needed to better constrain P-enabled models.

721

722

## 723 **4.5. Effects of accounting for the P cycle dynamics on simulated carbon balance**

### 724 **4.5.1. Spatial variation of nutrient limitation**

725 Our simulated nutrient limitation pattern broadly agrees with the findings from Elser et  
726 al. (2007) which supports the generally accepted notion that tropical ecosystems residing  
727 on highly weathered soils are P limited (Walker and Syers, 1976; Lebauer and Treseder,  
728 2008). A recent study that predicted spatial patterns of N and P limitation using the ratios  
729 of leaf N and P resorption efficiencies also found a shift from P limitation to N limitation  
730 with increasing latitude (Du et al., 2020). Lebauer and Treseder (2008) showed that N  
731 limitation is widespread, even in tropical regions. This is consistent with our model  
732 simulations which show that although P is more limiting in tropical forests, N is also a  
733 limiting nutrient. The geographic distribution of nutrient limitation is generally in  
734 agreement with that from Goll et al. (2012) and Wang et al. (2010). Goll et al. (2012)  
735 suggests that P limits C uptake mainly in low latitude regions and high latitudes, while N is

736 the limiting nutrient in temperate regions. It is worth mentioning that in Goll et al. (2012) N  
737 and P limitation generally have distinct geographic occurrence while this study suggests NP  
738 co-limitation occurs in many parts of the world. Wang et al. (2010) also showed that  
739 productivity in tropical forests and savanna is limiting by P, while most other biomes are  
740 limited by N. This is broadly consistent with our results but with a few key differences.  
741 Wang et al. (2010) suggests that P is the limiting nutrient for savannas, whereas our results  
742 show savannas are more limited by N. This may have to do with the lack of representation  
743 of fire disturbance in Wang et al. (2010). Savannas are subject to regular wildfires, which  
744 could have significant effects on nutrient cycle dynamics and nutrient limitation. For  
745 example, it has been suggested that while combustion causes significant gaseous losses of  
746 N from burned ecosystems, P is largely retained as ash (Herbert et al., 2003). Braakhekke et  
747 al (2017) also showed that there are strong losses of N due to fire. Furthermore, Wang et  
748 al. (2010) suggested that tropical forests are limited only by P, not by N, whereas our  
749 results indicate that N and P both limit tropical forest productivity, although P limitation is  
750 more dominant in most of the lowland tropical forests. This is consistent with a recent  
751 meta-analysis of nutrient fertilization experiments in tropical forests (Wright et al., 2018).

752

#### 753 **4.5.2. The implications for global carbon cycle and climate**

754 Historical C accumulation is a result of many complex and sometimes counteracting  
755 processes controlling C fluxes and stocks (Lawrence et al., 2019), including accumulation of  
756 carbon on land due to CO<sub>2</sub> fertilization, accumulation due to nitrogen deposition, carbon  
757 fluxes due to climate variability and climate change, and losses and gains due to land cover  
758 conversion and regrowth following historical land cover changes (LULCC fluxes). Over the  
759 long term, two of the dominant processes controlling C accumulation in terrestrial  
760 ecosystems are C emissions due to LULCC and C uptake due to the CO<sub>2</sub> fertilization effect. P  
761 cycle dynamics have important impacts on both of these processes, but with opposite sign.  
762 Globally, considering P cycle dynamics leads to lower carbon emissions associated with  
763 deforestation by about 11% (161.21 Pg in CN vs 143.89 in CNP). Conversely, CO<sub>2</sub>  
764 fertilization at the global scale is reduced by 20% when P limitation is included during the

765 historical time period (134 Pg C vs 108 Pg C). In general, the ELMv1-CN simulation shows a  
766 CO<sub>2</sub> fertilization effect on biomass that is too strong, which leads to a stronger than  
767 observed carbon sink compared to observational constraints from both Hoffman et al.  
768 (2014) and Le Quere et al. (2016). ELMv1-CN simulation also produces stronger carbon  
769 emissions from LULCC due to having higher biomass compared to ELMv1-CNP. The CO<sub>2</sub>  
770 fertilization effect in the ELMv1-CN simulations is strong enough to overcome the LULCC  
771 losses with the net result being too large of a sink throughout the historical time period for  
772 the CN model. Both model configurations lose carbon too slowly due to LULCC in the period  
773 from 1850–1940, when compared to the Hoffman et al. (2014) global estimate. Both  
774 models also predict continued losses over the period 1940–1965, while the Hoffman et al.  
775 (2014) estimate switches from net carbon loss to net carbon accumulation around 1940.  
776 These are clearly shown in Fig. S9, which shows the time series of simulated change in land  
777 carbon storage in response to changes in CO<sub>2</sub>, LULCC, N deposition, and climate during  
778 1850-2010. The ELMv1-CN and ELMv1-CNP models are similar to many other CMIP6  
779 models with respect to this bias in the timing of transition from net land carbon source to  
780 net land sink as shown in our ILAMB analysis of other land models in CMIP6.

781  
782 We also note that, over the historical time period, P became more limiting as simulated  
783 historical C accumulations became increasingly divergent between CN and CNP simulations.  
784 This is mainly caused by stimulated plant productivity under higher atmospheric CO<sub>2</sub>, which  
785 leads to higher plant demand for P that is not balanced by increased supply of newly  
786 mineralized P from the soil. This is consistent with other global modeling studies with  
787 explicit representation of P cycle dynamics (Goll et al., 2012; Zhang et al., 2014), as well as  
788 diagnostic studies that evaluated how CO<sub>2</sub> fertilization simulated by CMIP5 models could  
789 be constrained by soil P availability using a mass balance approach (Wieder et al., 2015b;  
790 Sun et al., 2017). Taken together, the limiting effect of P availability on C uptake will likely  
791 have substantial consequences for projections of future C uptake.

792  
793

794 **4.6. Limitations and future development**

795 While the ELMv1-CNP simulations presented here show that the model is capable of  
796 representing contemporary C, N and P stocks and fluxes and capturing the observed  
797 ecosystem responses to changes in atmospheric CO<sub>2</sub>, the current configuration does have  
798 limitations.

799 While the model represents disturbances such as fire and the interactions between  
800 disturbances and nutrient cycle dynamics, these interactions and how they affect carbon  
801 cycle processes have not been well constrained with observational data. There is a growing  
802 body of literature investigating the biogeochemical signature of fire. For example, a meta-  
803 analysis by Butler et al. (2018) shows that fire led to significantly higher concentration of  
804 soil mineral P and lower soil and litter C:P and N:P ratios, therefore decoupling the P cycle  
805 from the C and N cycles. We will take advantage of these recent findings to improve model  
806 fidelity on this front.

807 Another area that needs to be improved is the treatment of N fixation and how that is  
808 linked to P availability. N fixation in ELMv1-CNP is represented as a function of NPP  
809 (Cleveland et al., 1999). While providing a reasonable global estimate of N fixation, the  
810 approach ignores existing mechanistic understanding of nitrogen fixation processes  
811 (Wieder et al., 2015a). Furthermore, several lines of evidence suggest that both symbiotic  
812 and free-living N fixation rates depend on the availability of other elements, such as P and  
813 molybdenum (Reed et al., 2013; Nasto et al., 2014). N fixation could have important  
814 implications for the spatial distribution of N limitation vs P limitation. In the future we plan  
815 to have a more mechanistic representation of N fixation in ELM.

816 In ELMv1-CNP, P limitation is represented by downregulating plant growth when P  
817 demand is greater than soil P availability. The mechanisms by which P fundamentally limits  
818 ecosystem productivity remain uncertain (Jiang et al., 2019). Some studies proposed that  
819 there are linear or log-linear relationships between leaf P concentration and  
820 photosynthetic parameters, although the relationship has been shown to be weak (Walker  
821 et al., 2014). P fertilization experiments in P limited ecosystems do not support this  
822 proposed relationship. A P fertilization experiment on highly weathered soils in Australia

823 showed that although leaf P concentration increased significantly (+50%) compared to  
824 unfertilized trees, photosynthetic capacity was unaffected (Crous et al., 2015).  
825 Another fertilization experiment in Hawaii showed that the increase of aboveground NPP  
826 with P fertilization was caused mainly by increases in LAI instead of photosynthesis per unit  
827 leaf area (Herbert and Fownes, 1995). Further laboratory and field experiments are needed  
828 to help us better understand and represent the role of P in photosynthesis. Investigating  
829 the detailed mechanisms through which leaf P concentration affects photosynthesis is an  
830 active field of research (Jiang et al., 2019; Norby et al., 2017; Crous et al., 2015), and  
831 representing these relationships in land models remains an outstanding challenge.

832       Uncertainty also remains regarding the ELMv1-CNP representation of sorption dynamics  
833 and biochemical mineralization and their responses to changes in atmospheric CO<sub>2</sub> and  
834 climate (Fleischer et al., 2019). Motivated by our previous modeling studies, several recent  
835 field studies have started focusing on improving our mechanistic understanding and  
836 providing quantitative relationships for modelling these processes (Cabugao et al., 2017;  
837 Brenner et al., 2019). A recent study that upscaled site-measurements of potential  
838 phosphatase activity to continental Europe using machine learning technique provides a  
839 potential pathway toward generating benchmark data for biochemical mineralization on  
840 regional to global scale (Sun et al., 2020). ELMv1-CNP is likely underestimating P leaching,  
841 in comparison to the estimate of Wang et al. (2018), which could contribute to the  
842 underestimate of P uptake and overestimate of land carbon sink. We will further improve  
843 the representation of P leaching in ELMv1. There are other mechanisms that could sustain  
844 productivity with increasing P limitation but were not considered in ELMv1-CNP, such as  
845 flexible stoichiometry and dynamic allocation. These will be investigated further in future  
846 versions of E3SM. However, as Fleischer et al. (2019) pointed out, since plant N:P ratios in  
847 highly P limited tropical forests are already at the high end of the observed spectrum, the  
848 role of stoichiometry plasticity in sustaining tropical productivity could be limited.

849       While the representation of NSC has helped ELMv1-CNP to capture the interannual  
850 variability of atmospheric CO<sub>2</sub> and to generate ecosystem responses to elevated CO<sub>2</sub>  
851 consistent with FACE measurements, the sizes and turnover times of NSC pools are not well

852 constrained. We will synthesize limited measurements on NSC from literature that include  
853 observational and experimental data as well as measurements from isotopic studies to  
854 better understand the dynamics of the NSC pool and to evaluate and refine its  
855 representation in ELM. We also advocate for more measurements on NSC and how they  
856 respond to environmental changes in diverse ecosystems to have a more complete  
857 understanding and quantification of NSC.

858 Finally, although models such as ELMv1-CNP and CLM5 perform similarly when  
859 evaluated against present-day metrics as gathered in ILAMB, we expect that the  
860 differences among models in their representation of observed processes and in their  
861 assumptions about how changes in atmospheric composition and climate will impact  
862 ecosystem processes will lead to diverging predictions under future climate scenarios. We  
863 will explore those differences and their consequences in future work.

864

## 865 **5. Conclusions**

866 In this study, we provide an evaluation of ELMv1-CNP using the ILAMB benchmarking  
867 system, comparison with CO<sub>2</sub> manipulation experiments, and comparison with other  
868 observational and modeling studies. Benchmarking with ILAMB indicates ELMv1-CNP  
869 produces realistic estimates of present-day carbon pools and fluxes. Compared to a  
870 simulation with optimal P availability, ELMv1-CNP produces better performance,  
871 particularly for the metrics that are most relevant to land-atmosphere exchange. Our  
872 results from CO<sub>2</sub> manipulation experiments suggest that ELMv1-CNP is able to capture  
873 observed responses to elevated CO<sub>2</sub>, including those for GPP, NPP, vegetation C, and LAI.  
874 Further analysis suggests that the introduction of a non-structural carbon pool in ELMv1-  
875 CNP is largely responsible for these improvements. Evaluating global C, N, and P pools and  
876 fluxes in the context of literature values suggests that ELMv1-CNP provides a reasonable  
877 representation of contemporary global scale C, N and P cycles.

878 We highlight the data needs for global land model evaluation, particularly the need for  
879 more synthesis datasets on nutrient pools and fluxes, as well as observations from  
880 manipulation experiments that provide additional benchmark data for nutrient cycle

881 evaluation. This need is becoming increasingly pressing as more land models are including N  
882 and P cycle dynamics and C-N-P interactions. We also identify challenges in constraining P  
883 cycle dynamics and point to the need for soil P measurements.

884 Our simulations suggest, probably not surprisingly, that in general P is the more limiting  
885 nutrient in the tropical regions while N is more limiting in the middle to high latitudes.  
886 However, our results also suggest widespread N and P colimitation, even in the tropical  
887 regions where P limitation is more dominant. Our results show that C sources and sinks are  
888 significantly affected by P limitation, as the historical CO<sub>2</sub> fertilization effect was reduced by  
889 20% and C emission due to LULCC was 11% lower when P limitation was considered. We  
890 conclude that introduction of P cycle dynamics and C-N-P coupling will likely have  
891 substantial consequences for projections of future C uptake.

892

#### 893 Acknowledgement:

894 This research was supported as part of the Energy Exascale Earth System Model (E3SM) project,  
895 funded by the U.S. Department of Energy, Office of Science, Office of Biological and  
896 Environmental Research. This research was also supported by the Oak Ridge National  
897 Laboratory's (ORNL) Terrestrial Ecosystem Science Focus Area (TES SFA). F. M. Hoffman was  
898 supported by the Reducing Uncertainties in Biogeochemical Interactions through Synthesis and  
899 Computation Scientific Focus Area (RUBISCO SFA), which is sponsored by the Regional and  
900 Global Model Analysis (RGMA) Program in the Climate and Environmental Sciences Division  
901 (CESD) of the Office of Biological and Environmental Research (BER) in the U.S. Department of  
902 Energy Office of Science. We thank Min Xu for his help in running ILAMB. The E3SM model can  
903 be accessed at <https://www.osti.gov/doecode/biblio/10475> (doi:  
904 [10.11578/E3SM/dc.20180418.36](https://doi.org/10.11578/E3SM/dc.20180418.36)). The input data is available at  
905 <https://web.lcrc.anl.gov/public/e3sm/inputdata/>.

906 The model outputs used in this study can be downloaded at the website:  
907 <https://doi.org/10.6084/m9.figshare.12021348>.

908

909

#### 910 References:

911 Ainsworth, E. A. and Long, S. P.: What have we learned from 15 years of free-air CO<sub>2</sub>  
912 enrichment (FACE)? A meta-analytic review of the responses of photosynthesis, canopy  
913 properties and plant production to rising CO<sub>2</sub>, *New phytologist*, 165, 351-372, 2005.  
914 Aragão, L., Malhi, Y., Metcalfe, D., Silva-Espejo, J., Jimenez, E., Navarrete, D., Almeida, S.,  
915 Costa, A., Salinas, N., and Phillips, O.: Above-and below-ground net primary productivity across  
916 ten Amazonian forests on contrasting soils, *Biogeosciences*, 6, 2759-2778, 2009.

917 Arora, V. K., Boer, G. J., Friedlingstein, P., Eby, M., Jones, C. D., Christian, J. R., Bonan, G.,  
918 Bopp, L., Brovkin, V., and Cadule, P.: Carbon-concentration and carbon-climate feedbacks in  
919 CMIP5 Earth system models, *Journal of Climate*, 26, 5289-5314, 2013.

920 Arora, V. K., Katavouta, A., Williams, R. G., Jones, C. D., Brovkin, V., Friedlingstein, P.,  
921 Schwinger, J., Bopp, L., Boucher, O., and Cadule, P.: Carbon-concentration and carbon-climate  
922 feedbacks in CMIP6 models and their comparison to CMIP5 models, *Biogeosciences*, 17, 4173-  
923 4222, 2020.

924 Avitabile, V., Herold, M., Heuvelink, G. B., Lewis, S. L., Phillips, O. L., Asner, G. P., Armston,  
925 J., Ashton, P. S., Banin, L., and Bayol, N.: An integrated pan-tropical biomass map using  
926 multiple reference datasets, *Global change biology*, 22, 1406-1420, 2016.

927 Baig, S., Medlyn, B. E., Mercado, L. M., and Zaehle, S.: Does the growth response of woody  
928 plants to elevated CO<sub>2</sub> increase with temperature? A model-oriented meta-analysis, *Global  
929 change biology*, 21, 4303-4319, 2015.

930 Barron, A. R., Wurzburger, N., Bellenger, J. P., Wright, S. J., Kraepiel, A. M., and Hedin, L. O.:  
931 Molybdenum limitation of asymbiotic nitrogen fixation in tropical forest soils, *Nature  
932 Geoscience*, 2, 42-45, 2008.

933 Batjes, N. H.: Total carbon and nitrogen in the soils of the world, *European journal of soil  
934 science*, 65, 10-21, 2014.

935 Beer, C., Reichstein, M., Tomelleri, E., Ciais, P., Jung, M., Carvalhais, N., Rödenbeck, C.,  
936 Arain, M. A., Baldocchi, D., and Bonan, G. B.: Terrestrial gross carbon dioxide uptake: global  
937 distribution and covariation with climate, *Science*, 329, 834-838, 2010.

938 Bonan, G. B., Lombardozzi, D. L., Wieder, W. R., Oleson, K. W., Lawrence, D. M., Hoffman, F.  
939 M., and Collier, N.: Model structure and climate data uncertainty in historical simulations of the  
940 terrestrial carbon cycle (1850–2014), *Global Biogeochemical Cycles*, 33, 1310-1326, 2019.

941 Bonan, G. B., Lawrence, P. J., Oleson, K. W., Levis, S., Jung, M., Reichstein, M., Lawrence, D.  
942 M., and Swenson, S. C.: Improving canopy processes in the Community Land Model version 4  
943 (CLM4) using global flux fields empirically inferred from FLUXNET data, *Journal of  
944 Geophysical Research: Biogeosciences*, 116, 2011.

945 Brenner, J., Porter, W., Phillips, J. R., Childs, J., Yang, X., and Mayes, M. A.: Phosphorus  
946 sorption on tropical soils with relevance to Earth system model needs, *Soil research*, 57, 17-27,  
947 2019.

948 Burrows, S., Maltrud, M., Yang, X., Zhu, Q., Jeffery, N., Shi, X., Ricciuto, D., Wang, S., Bisht,  
949 G., and Tang, J.: The DOE E3SM v1.1 Biogeochemistry Configuration: Description and  
950 Simulated Ecosystem-Climate Responses to Historical Changes in Forcing, *Journal of Advances  
951 in Modeling Earth Systems*, 12, e2019MS001766, 2020.

952 Butler, O. M., Elser, J. J., Lewis, T., Mackey, B., and Chen, C.: The phosphorus-rich signature of  
953 fire in the soil-plant system: a global meta-analysis, *Ecology letters*, 21, 335-344, 2018.

954 Cabugao, K. G., Timm, C. M., Carrell, A. A., Childs, J., Lu, T.-Y. S., Pelletier, D. A., Weston,  
955 D. J., and Norby, R. J.: Root and rhizosphere bacterial phosphatase activity varies with tree  
956 species and soil phosphorus availability in Puerto Rico tropical forest, *Frontiers in plant science*,  
957 8, 1834, 2017.

958 Campbell, J., Berry, J., Seibt, U., Smith, S. J., Montzka, S., Launois, T., Belviso, S., Bopp, L.,  
959 and Laine, M.: Large historical growth in global terrestrial gross primary production, *Nature*,  
960 544, 84-87, 2017.



961 Cleveland, C., Townsend, A., Schimel, D., Fisher, H., Howarth, R., Hedin, L., Perakis, S., Latty,  
 962 E., Von Fischer, J., and Elseroad, A.: Global patterns of terrestrial biological nitrogen (N<sub>2</sub>)  
 963 fixation in natural ecosystems, *Global Biogeochemical Cycles*, 13, 623-645, 1999.  
 964 Collier, N., Hoffman, F. M., Lawrence, D. M., Keppel-Aleks, G., Koven, C. D., Riley, W. J.,  
 965 Mu, M., and Randerson, J. T.: The International Land Model Benchmarking (ILAMB) system:  
 966 design, theory, and implementation, *Journal of Advances in Modeling Earth Systems*, 10, 2731-  
 967 2754, 2018.  
 968 Crews, T. E., Farrington, H., and Vitousek, P. M.: Changes in asymbiotic, heterotrophic nitrogen  
 969 fixation on leaf litter of *Metrosideros polymorpha* with long-term ecosystem development in  
 970 Hawaii, *Ecosystems*, 3, 386-395, 2000.  
 971 Crous, K. Y., Osvaldsson, A., and Ellsworth, D. S.: Is phosphorus limiting in a mature  
 972 *Eucalyptus* woodland? Phosphorus fertilisation stimulates stem growth, *Plant and soil*, 391, 293-  
 973 305, 2015.  
 974 Davies-Barnard, T. and Friedlingstein, P.: The Global Distribution of Biological Nitrogen  
 975 Fixation in Terrestrial Natural Ecosystems, *Global Biogeochemical Cycles*, 34,  
 976 e2019GB006387, 10.1029/2019gb006387, 2020.  
 977 Davies-Barnard, T., Meyerholt, J., Zaehle, S., Friedlingstein, P., Brovkin, V., Fan, Y., Fisher, R.  
 978 A., Jones, C. D., Lee, H., and Peano, D.: Nitrogen cycling in CMIP6 land surface models:  
 979 Progress and limitations, *Biogeosciences Discussions*, 2020.  
 980 DeFries, R., Field, C., Fung, I., Collatz, G., and Bounoua, L.: Combining satellite data and  
 981 biogeochemical models to estimate global effects of human-induced land cover change on  
 982 carbon emissions and primary productivity, *Global biogeochemical cycles*, 13, 803-815, 1999.  
 983 Du, E., Terrer, C., Pellegrini, A. F., Ahlström, A., van Lissa, C. J., Zhao, X., Xia, N., Wu, X.,  
 984 and Jackson, R. B.: Global patterns of terrestrial nitrogen and phosphorus limitation, *Nature*  
 985 *Geoscience*, 13, 221-226, 2020.  
 986 Duarte, H. F., Raczka, B. M., Ricciuto, D. M., Lin, J. C., Koven, C. D., Thornton, P. E.,  
 987 Bowling, D. R., Lai, C.-T., Bible, K. J., and Ehleringer, J. R.: Evaluating the Community Land  
 988 Model (CLM4. 5) at a coniferous forest site in northwestern United States using flux and carbon-  
 989 isotope measurements, *Biogeosciences (Online)*, 14, 2017.  
 990 Edwards, E., McCaffery, S., and Evans, J.: Phosphorus availability and elevated CO<sub>2</sub> affect  
 991 biological nitrogen fixation and nutrient fluxes in a clover dominated sward, *New Phytologist*,  
 992 169, 157-167, 2006.  
 993 Ehlers, I., Augusti, A., Betson, T. R., Nilsson, M. B., Marshall, J. D., and Schleucher, J.:  
 994 Detecting long-term metabolic shifts using isotopomers: CO<sub>2</sub>-driven suppression of  
 995 photorespiration in C<sub>3</sub> plants over the 20th century, *Proceedings of the National Academy of*  
 996 *Sciences*, 112, 15585-15590, 2015.  
 997 Ellsworth, D. S., Anderson, I. C., Crous, K. Y., Cooke, J., Drake, J. E., Gherlenda, A. N.,  
 998 Gimeno, T. E., Macdonald, C. A., Medlyn, B. E., and Powell, J. R.: Elevated CO<sub>2</sub> does not  
 999 increase eucalypt forest productivity on a low-phosphorus soil, *Nature Climate Change*, 7, 279-  
 1000 282, 2017.  
 1001 Elser, J. J., Bracken, M. E. S., Cleland, E. E., Gruner, D. S., Harpole, W. S., Hillebrand, H.,  
 1002 Ngai, J. T., Seabloom, E. W., Shurin, J. B., and Smith, J. E.: Global analysis of nitrogen and  
 1003 phosphorus limitation of primary producers in freshwater, marine and terrestrial ecosystems,  
 1004 *Ecology Letters*, 10, 1135-1142, 10.1111/j.1461-0248.2007.01113.x, 2007.

1005 Erb, K.-H., Kastner, T., Plutzer, C., Bais, A. L. S., Carvalhais, N., Fetzel, T., Gingrich, S.,  
1006 Haberl, H., Lauk, C., and Niedertscheider, M.: Unexpectedly large impact of forest management  
1007 and grazing on global vegetation biomass, *Nature*, 553, 73-76, 2018.

1008 Finzi, A. C., Norby, R. J., Calfapietra, C., Gallet-Budynek, A., Gielen, B., Holmes, W. E.,  
1009 Hoosbeek, M. R., Iversen, C. M., Jackson, R. B., and Kubiske, M. E.: Increases in nitrogen  
1010 uptake rather than nitrogen-use efficiency support higher rates of temperate forest productivity  
1011 under elevated CO<sub>2</sub>, *Proceedings of the National Academy of Sciences*, 104, 14014-14019,  
1012 2007.

1013 Fleischer, K., Rammig, A., De Kauwe, M. G., Walker, A. P., Domingues, T. F., Fuchslueger, L.,  
1014 Garcia, S., Goll, D. S., Grandis, A., and Jiang, M.: Amazon forest response to CO<sub>2</sub> fertilization  
1015 dependent on plant phosphorus acquisition, *Nature Geoscience*, 12, 736-741, 2019.

1016 Friedlingstein, P., Jones, M., O'Sullivan, M., Andrew, R., Hauck, J., Peters, G., Peters, W.,  
1017 Pongratz, J., Sitch, S., and Le Quéré, C.: Global carbon budget 2019, *Earth System Science Data*,  
1018 11, 1783-1838, 2019.

1019 Gerber, S., Hedin, L. O., Oppenheimer, M., Pacala, S. W., and Shevliakova, E.: Nitrogen cycling  
1020 and feedbacks in a global dynamic land model, *Global Biogeochemical Cycles*, 24, GB1001,  
1021 10.1029/2008gb003336, 2010.

1022 Ghimire, B., Riley, W. J., Koven, C. D., Mu, M., and Randerson, J. T.: Representing leaf and  
1023 root physiological traits in CLM improves global carbon and nitrogen cycling predictions,  
1024 *Journal of Advances in Modeling Earth Systems*, 8, 598-613, 2016.

1025 Goll, D., Winkler, A., Raddatz, T., Dong, N., Prentice, I., Ciais, P., and Brovkin, V.: Carbon–  
1026 nitrogen interactions in idealized simulations with JSBACH (version 3.10), *Geosci. Model Dev.*,  
1027 10, 2009–2030, 2017a.

1028 Goll, D., Brovkin, V., Parida, B., Reick, C., Kattge, J., Reich, P., van Bodegom, P., and  
1029 Niinemets, U.: Nutrient limitation reduces land carbon uptake in simulations with a model of  
1030 combined carbon, nitrogen and phosphorus cycling, *Biogeosciences*, 9, 3547-3569, 2012.

1031 Goll, D., Vuichard, N., Maignan, F., Jornet-Puig, A., Sardans, J., Violette, A., Peng, S., Sun, Y.,  
1032 Kvakic, M., and Guimberteau, M.: A representation of the phosphorus cycle for ORCHIDEE  
1033 (revision 4520), 2017b.

1034 Haverd, V., Smith, B., Canadell, J. G., Cuntz, M., Mikaloff-Fletcher, S., Farquhar, G.,  
1035 Woodgate, W., Briggs, P. R., and Trudinger, C. M.: Higher than expected CO<sub>2</sub> fertilization  
1036 inferred from leaf to global observations, *Global change biology*, 26, 2390-2402, 2020.

1037 Herbert, D. A. and Fownes, J. H.: Phosphorus limitation of forest leaf area and net primary  
1038 production on a highly weathered soil, *Biogeochemistry*, 29, 223-235, 1995.

1039 Herbert, D. A., Williams, M., and Rastetter, E. B.: A model analysis of N and P limitation on  
1040 carbon accumulation in Amazonian secondary forest after alternate land-use abandonment,  
1041 *Biogeochemistry*, 65, 121-150, 2003.

1042 Hoffman, F., Koven, C., Keppel-Aleks, G., Lawrence, D., Riley, W., Randerson, J., Ahlström,  
1043 A., Abramowitz, G., Baldocchi, D., and Best, M.: International land model benchmarking  
1044 (ILAMB) 2016 Workshop Report, US Department of Energy, Office of Science, 10, 1330803,  
1045 2017.

1046 Hoffman, F. M., Randerson, J. T., Arora, V. K., Bao, Q., Cadule, P., Ji, D., Jones, C. D.,  
1047 Kawamiya, M., Khatiwala, S., and Lindsay, K.: Causes and implications of persistent  
1048 atmospheric carbon dioxide biases in Earth System Models, *Journal of Geophysical Research:*  
1049 *Biogeosciences*, 119, 141-162, 2014.

1050 Hou, E., Tan, X., Heenan, M., and Wen, D.: A global dataset of plant available and unavailable  
1051 phosphorus in natural soils derived by Hedley method, *Scientific data*, 5, 180166, 2018.

1052 Hou, E., Luo, Y., Kuang, Y., Chen, C., Lu, X., Jiang, L., Luo, X., and Wen, D.: Global meta-  
1053 analysis shows pervasive phosphorus limitation of aboveground plant production in natural  
1054 terrestrial ecosystems, *Nature Communications*, 11, 1-9, 2020.

1055 Houghton, R. A.: The contemporary carbon cycle, *Treatise on geochemistry*, 8, 473-513, 2003.

1056 Houlton, B. Z., Wang, Y.-P., Vitousek, P. M., and Field, C. B.: A unifying framework for  
1057 dinitrogen fixation in the terrestrial biosphere, *Nature*, 454, 327-330, 10.1038/nature07028,  
1058 2008.

1059 Huete, A., Didan, K., Miura, T., Rodriguez, E. P., Gao, X., and Ferreira, L. G.: Overview of the  
1060 radiometric and biophysical performance of the MODIS vegetation indices, *Remote sensing of*  
1061 *environment*, 83, 195-213, 2002.

1062 Hungate, B. A., Dukes, J. S., Shaw, M. R., Luo, Y., and Field, C. B.: Nitrogen and climate  
1063 change, *Science*, 302, 1512-1513, 2003.

1064 Hungate, B. A., Stiling, P. D., Dijkstra, P., Johnson, D. W., Ketterer, M. E., Hymus, G. J.,  
1065 Hinkle, C. R., and Drake, B. G.: CO<sub>2</sub> elicits long-term decline in nitrogen fixation, *Science*, 304,  
1066 1291, 2004.

1067 Jahnke, R.: The phosphorus cycle, *Global Biogeochemical Cycles*, 301-315, 1992.

1068 Jiang, M., Caldararu, S., Zaehle, S., Ellsworth, D. S., and Medlyn, B. E.: Towards a more  
1069 physiological representation of vegetation phosphorus processes in land surface models, *New*  
1070 *Phytologist*, 222, 1223-1229, 2019.

1071 Jobbágy, E. G. and Jackson, R. B.: The vertical distribution of soil organic carbon and its relation  
1072 to climate and vegetation, *Ecological applications*, 10, 423-436, 2000.

1073 Joiner, J., Yoshida, Y., Zhang, Y., Duveiller, G., Jung, M., Lyapustin, A., Wang, Y., and Tucker,  
1074 C. J.: Estimation of terrestrial global gross primary production (GPP) with satellite data-driven  
1075 models and eddy covariance flux data, *Remote Sensing*, 10, 1346, 2018.

1076 Jones, C. D., Arora, V., Friedlingstein, P., Bopp, L., Brovkin, V., Dunne, J., Graven, H.,  
1077 Hoffman, F., Ilyina, T., and John, J. G.: C4MIP—The coupled climate–carbon cycle model  
1078 intercomparison project: Experimental protocol for CMIP6, *Geoscientific Model Development*,  
1079 9, 2853-2880, 2016.

1080 Jung, C.-G., Shin, H.-J., Park, M.-J., Joh, H.-K., and Kim, S.-J.: Evaluation of MODIS Gross  
1081 Primary Production (GPP) by Comparing with GPP from CO<sub>2</sub> Flux Data Measured in a Mixed  
1082 Forest Area, *Journal of the Korean Society of Agricultural Engineers*, 53, 1-8, 2011.

1083 Kobayashi, H. and Dye, D. G.: Atmospheric conditions for monitoring the long-term vegetation  
1084 dynamics in the Amazon using normalized difference vegetation index, *Remote Sensing of*  
1085 *Environment*, 97, 519-525, 2005.

1086 Köchy, M., Hiederer, R., and Freibauer, A.: Global distribution of soil organic carbon—Part 1:  
1087 Masses and frequency distributions of SOC stocks for the tropics, permafrost regions, wetlands,  
1088 and the world, *Soil*, 1, 351-365, 2015.

1089 Koven, C., Riley, W., Subin, Z., Tang, J., Torn, M., Collins, W., Bonan, G., Lawrence, D., and  
1090 Swenson, S.: The effect of vertically resolved soil biogeochemistry and alternate soil C and N  
1091 models on C dynamics of CLM4, *Biogeosciences*, 10, 7109, 2013.

1092 Lawrence, D. M., Fisher, R. A., Koven, C. D., Oleson, K. W., Swenson, S. C., Bonan, G.,  
1093 Collier, N., Ghimire, B., van Kampenhout, L., and Kennedy, D.: The Community Land Model  
1094 version 5: Description of new features, benchmarking, and impact of forcing uncertainty, *Journal*  
1095 *of Advances in Modeling Earth Systems*, 2019.

1096 Le Quéré, C., Andrew, R., Canadell, J. G., Sitch, S., Korsbakken, J. I., Peters, G. P., Manning, A.  
1097 C., Boden, T. A., Tans, P. P., and Houghton, R. A.: Global carbon budget 2016, 2016.

1098 Le Quéré, C., Andrew, R. M., Friedlingstein, P., Sitch, S., Hauck, J., Pongratz, J., Pickers, P. A.,  
1099 Korsbakken, J. I., Peters, G. P., and Canadell, J. G.: Global carbon budget 2018, *Earth System*  
1100 *Science Data*, 10, 2141-2194, 2018.

1101 LeBauer, D. S. and Treseder, K. K.: Nitrogen limitation of net primary productivity in terrestrial  
1102 ecosystems is globally distributed, *Ecology*, 89, 371-379, 2008.

1103 Lin, B.-L., Sakoda, A., Shibasaki, R., Goto, N., and Suzuki, M.: Modelling a global  
1104 biogeochemical nitrogen cycle in terrestrial ecosystems, *Ecological Modelling*, 135, 89-110,  
1105 2000.

1106 Luo, Y., Randerson, J. T., Friedlingstein, P., Hibbard, K., Hoffman, F., Huntzinger, D., Jones, C.,  
1107 Koven, C., Lawrence, D., and Li, D.: A framework for benchmarking land models, 2012.

1108 Mao, J., Ricciuto, D. M., Thornton, P. E., Warren, J. M., King, A. W., Shi, X., Iversen, C. M.,  
1109 and Norby, R. J.: Evaluating the Community Land Model in a pine stand with shading  
1110 manipulations and <sup>13</sup>CO<sub>2</sub> labeling, *Biogeosciences (Online)*, 13, 2016.

1111 Marklein, A. R. and Houlton, B. Z.: Nitrogen inputs accelerate phosphorus cycling rates across a  
1112 wide variety of terrestrial ecosystems, *New Phytologist*, 193, 696-704, 2012.

1113 Matthews, E.: Global litter production, pools, and turnover times: Estimates from measurement  
1114 data and regression models, *Journal of Geophysical Research: Atmospheres*, 102, 18771-18800,  
1115 1997.

1116 McGill, W. and Cole, C.: Comparative aspects of cycling of organic C, N, S and P through soil  
1117 organic matter, *Geoderma*, 26, 267-286, 1981.

1118 Melillo, J., Steudler, P., Aber, J., Newkirk, K., Lux, H., Bowles, F., Catricala, C., Magill, A.,  
1119 Ahrens, T., and Morrisseau, S.: Soil warming and carbon-cycle feedbacks to the climate system,  
1120 *Science*, 298, 2173-2176, 2002.

1121 Metcalfe, D. B., Ricciuto, D., Palmroth, S., Campbell, C., Hurry, V., Mao, J., Keel, S. G., Linder,  
1122 S., Shi, X., and Näsholm, T.: Informing climate models with rapid chamber measurements of  
1123 forest carbon uptake, *Global change biology*, 23, 2130-2139, 2017.

1124 Mitchard, E. T., Feldpausch, T. R., Brienen, R. J., Lopez-Gonzalez, G., Monteagudo, A., Baker,  
1125 T. R., Lewis, S. L., Lloyd, J., Quesada, C. A., and Gloor, M.: Markedly divergent estimates of A  
1126 mazon forest carbon density from ground plots and satellites, *Global Ecology and Biogeography*,  
1127 23, 935-946, 2014.

1128 Nakhavali, M., Mercado, L. M., Hartley, I. P., Sitch, S., Cunha, F. V., di Ponzio, R., Lugli, L. F.,  
1129 Quesada, C. A., Andersen, K. M., and Chadburn, S. E.: Representation of phosphorus cycle in  
1130 Joint UK Land Environment Simulator (vn5. 5\_JULES-CNP), *Geoscientific Model*  
1131 *Development Discussions*, 1-24, 2021.

1132 Nasto, M. K., Alvarez-Clare, S., Lekberg, Y., Sullivan, B. W., Townsend, A. R., and Cleveland,  
1133 C. C.: Interactions among nitrogen fixation and soil phosphorus acquisition strategies in lowland  
1134 tropical rain forests, *Ecology Letters*, 17, 1282-1289, 2014.

1135 Norby, R. J., Gu, L., Haworth, I. C., Jensen, A. M., Turner, B. L., Walker, A. P., Warren, J. M.,  
1136 Weston, D. J., Xu, C., and Winter, K.: Informing models through empirical relationships  
1137 between foliar phosphorus, nitrogen and photosynthesis across diverse woody species in tropical  
1138 forests of Panama, *New Phytologist*, 215, 1425-1437, 2017.

1139 Olander, L. P. and Vitousek, P. M.: Regulation of soil phosphatase and chitinase activity by N  
1140 and P availability, *Biogeochemistry*, 49, 175-191, 2000.

1141 Oleson, K., Lawrence, D., Bonan, G., Drewniak, B., Huang, M., Koven, C., Levis, S., Li, F.,  
 1142 Riley, W., and Subin, Z.: Technical Description of version 4.5 of the Community Land Model  
 1143 (CLM)(NCAR Technical Note No. NCAR/TN-503+ STR). Citeseer, National Center for  
 1144 Atmospheric Research, PO Box, 3000, 2013.  
 1145 Pan, Y., Birdsey, R. A., Fang, J., Houghton, R., Kauppi, P. E., Kurz, W. A., Phillips, O. L.,  
 1146 Shvidenko, A., Lewis, S. L., and Canadell, J. G.: A large and persistent carbon sink in the  
 1147 world, *Science*, 333, 988-993, 2011.  
 1148 Post, W. M., Pastor, J., Zinke, P. J., and Stangenberger, A. G.: Global patterns of soil nitrogen  
 1149 storage, *Nature*, 317, 613-616, 1985.  
 1150 Raczka, B., Duarte, H. F., Koven, C. D., Ricciuto, D., Thornton, P. E., Lin, J. C., and Bowling,  
 1151 D. R.: An observational constraint on stomatal function in forests: evaluating coupled carbon and  
 1152 water vapor exchange with carbon isotopes in the Community Land Model (CLM4. 5),  
 1153 *Biogeosciences*, 13, 5183-5204, 2016.  
 1154 Reed, S. C., Cleveland, C. C., and Townsend, A. R.: Relationships among phosphorus,  
 1155 molybdenum and free-living nitrogen fixation in tropical rain forests: results from observational  
 1156 and experimental analyses, *Biogeochemistry*, 1-13, 2013.  
 1157 Reed, S. C., Yang, X., and Thornton, P. E.: Incorporating phosphorus cycling into global  
 1158 modeling efforts: a worthwhile, tractable endeavor, *New Phytologist*, 208, 324-329, 2015.  
 1159 Santoro, M., Beaudoin, A., Beer, C., Cartus, O., Fransson, J. E., Hall, R. J., Pathe, C.,  
 1160 Schmullius, C., Schepaschenko, D., and Shvidenko, A.: Forest growing stock volume of the  
 1161 northern hemisphere: Spatially explicit estimates for 2010 derived from Envisat ASAR, *Remote  
 1162 Sensing of Environment*, 168, 316-334, 2015.  
 1163 Sellar, A. A., Jones, C. G., Mulcahy, J., Tang, Y., Yool, A., Wiltshire, A., O'connor, F. M.,  
 1164 Stringer, M., Hill, R., and Palmieri, J.: UKESM1: Description and evaluation of the UK Earth  
 1165 System Model, *Journal of Advances in Modeling Earth Systems*, 2019.  
 1166 Shabanov, N. V., Huang, D., Yang, W., Tan, B., Knyazikhin, Y., Myneni, R. B., Ahl, D. E.,  
 1167 Gower, S. T., Huete, A. R., and Aragão, L. E. O.: Analysis and optimization of the MODIS leaf  
 1168 area index algorithm retrievals over broadleaf forests, *IEEE Transactions on Geoscience and  
 1169 Remote Sensing*, 43, 1855-1865, 2005.  
 1170 Smil, V.: P Phosphorus in the Environment: Natural Flows and Human Interferences, *Annual  
 1171 review of energy and the environment*, 25, 53-88, 2000.  
 1172 Smith, B., Warlind, D., Arneeth, A., Hickler, T., Leadley, P., Siltberg, J., and Zaehle, S.:  
 1173 Implications of incorporating N cycling and N limitations on primary production in an  
 1174 individual-based dynamic vegetation model, *Biogeosciences*, 11, 2027-2054, 2014.  
 1175 Sun, Y., Goll, D. S., Ciais, P., Peng, S., Margalef, O., Asensio, D., Sardans, J., and Peñuelas, J.:  
 1176 Spatial pattern and environmental drivers of acid phosphatase activity in Europe, 2020.  
 1177 Sun, Y., Goll, D. S., Chang, J., Ciais, P., Guenet, B., Helfenstein, J., Huang, Y., Lauerwald, R.,  
 1178 Maignan, F., and Naipal, V.: Global evaluation of the nutrient-enabled version of the land  
 1179 surface model ORCHIDEE-CNP v1. 2 (r5986), *Geoscientific Model Development*, 14, 1987-  
 1180 2010, 2021.  
 1181 Sun, Y., Peng, S., Goll, D. S., Ciais, P., Guenet, B., Guimberteau, M., Hinsinger, P., Janssens, I.  
 1182 A., Peñuelas, J., and Piao, S.: Diagnosing phosphorus limitations in natural terrestrial ecosystems  
 1183 in carbon cycle models, *Earth's future*, 5, 730-749, 2017.  
 1184 Terrer, C., Jackson, R. B., Prentice, I. C., Keenan, T. F., Kaiser, C., Vicca, S., Fisher, J. B.,  
 1185 Reich, P. B., Stocker, B. D., and Hungate, B. A.: Nitrogen and phosphorus constrain the CO<sub>2</sub>  
 1186 fertilization of global plant biomass, *Nature Climate Change*, 9, 684-689, 2019.

1187 Thornton, P., Doney, S., Lindsay, K., Moore, J., Mahowald, N., Randerson, J., Fung, I.,  
1188 Lamarque, J., Feddema, J., and Lee, Y.: Carbon-nitrogen interactions regulate climate-carbon  
1189 cycle feedbacks: results from an atmosphere-ocean general circulation model, 2009.  
1190 Thornton, P. E., Lamarque, J.-F., Rosenbloom, N. A., and Mahowald, N. M.: Influence of  
1191 carbon-nitrogen cycle coupling on land model response to CO<sub>2</sub> fertilization and climate  
1192 variability, *Global Biogeochemical Cycles*, 21, GB4018, 10.1029/2006gb002868, 2007.  
1193 Thum, T., Caldararu, S., Engel, J., Kern, M., Pallandt, M., Schnur, R., Yu, L., and Zaehle, S.: A  
1194 new terrestrial biosphere model with coupled carbon, nitrogen, and phosphorus cycles (QUINCY  
1195 v1. 0; revision 1772), *Geoscientific Model Development*, 12, 4781-4802, 2019.  
1196 Todd-Brown, K., Randerson, J., Post, W., Hoffman, F., Tarnocai, C., Schuur, E., and Allison, S.:  
1197 Causes of variation in soil carbon simulations from CMIP5 Earth system models and comparison  
1198 with observations, *Biogeosciences*, 10, 1717-1736, 2013.  
1199 Treseder, K. K. and Vitousek, P. M.: Effects of soil nutrient availability on investment in  
1200 acquisition of N and P in Hawaiian rain forests, *Ecology*, 82, 946-954, 2001.  
1201 Van den Hurk, B., Kim, H., Krinner, G., Seneviratne, S. I., Derksen, C., Oki, T., Douville, H.,  
1202 Colin, J., Ducharne, A., and Cheruy, F.: LS3MIP (v1. 0) contribution to CMIP6: the Land  
1203 Surface, Snow and Soil moisture Model Intercomparison Project-aims, setup and expected  
1204 outcome, *Geoscientific Model Development*, 9, 2809-2832, 2016.  
1205 Vicca, S., Luysaert, S., Penuelas, J., Campioli, M., Chapin III, F., Ciais, P., Heinemeyer, A.,  
1206 Högberg, P., Kutsch, W., and Law, B. E.: Fertile forests produce biomass more efficiently,  
1207 *Ecology letters*, 15, 520-526, 2012.  
1208 Vitousek, P. M., Menge, D. N., Reed, S. C., and Cleveland, C. C.: Biological nitrogen fixation:  
1209 rates, patterns and ecological controls in terrestrial ecosystems, *Philosophical Transactions of the*  
1210 *Royal Society B: Biological Sciences*, 368, 20130119, 2013.  
1211 Vitousek, P. M., Porder, S., Houlton, B. Z., and Chadwick, O. A.: Terrestrial phosphorus  
1212 limitation: mechanisms, implications, and nitrogen-phosphorus interactions, *Ecological*  
1213 *applications*, 20, 5-15, 2010.  
1214 Walker, A. P., Beckerman, A. P., Gu, L., Kattge, J., Cernusak, L. A., Domingues, T. F., Scales,  
1215 J. C., Wohlfahrt, G., Wullschlegel, S. D., and Woodward, F. I.: The relationship of leaf  
1216 photosynthetic traits—V<sub>cmax</sub> and J<sub>max</sub>—to leaf nitrogen, leaf phosphorus, and specific leaf area: a  
1217 meta-analysis and modeling study, *Ecology and evolution*, 4, 3218-3235, 2014.  
1218 Walker, T. and Syers, J.: The fate of phosphorus during pedogenesis, *Geoderma*, 15, 1-19, 1976.  
1219 Wang, Y., Ciais, P., Goll, D. S., Huang, Y., Luo, Y., Wang, Y.-P., Bloom, A. A., Broquet, G.,  
1220 Hartmann, J., and Peng, S.: GOLUM-CNP v1. 0: a data-driven modeling of carbon, nitrogen and  
1221 phosphorus cycles in major terrestrial biomes, 2018.  
1222 Wang, Y.-P., Law, R. M., and Pak, B.: A global model of carbon, nitrogen and phosphorus  
1223 cycles for the terrestrial biosphere, *Biogeosciences*, 7, 2261-2282, 10.5194/bg-7-2261-2010,  
1224 2010.  
1225 Wang, Y. P., Houlton, B. Z., and Field, C. B.: A model of biogeochemical cycles of carbon,  
1226 nitrogen, and phosphorus including symbiotic nitrogen fixation and phosphatase production,  
1227 *Global Biogeochemical Cycles*, 21, GB1018, 10.1029/2006gb002797, 2007.  
1228 Welp, L. R., Keeling, R. F., Meijer, H. A., Bollenbacher, A. F., Piper, S. C., Yoshimura, K.,  
1229 Francey, R. J., Allison, C. E., and Wahlen, M.: Interannual variability in the oxygen isotopes of  
1230 atmospheric CO<sub>2</sub> driven by El Niño, *Nature*, 477, 579-582, 2011.

1231 Wieder, W. R., Cleveland, C. C., Lawrence, D. M., and Bonan, G. B.: Effects of model structural  
1232 uncertainty on carbon cycle projections: biological nitrogen fixation as a case study,  
1233 Environmental Research Letters, 10, 044016, 2015a.

1234 Wieder, W. R., Cleveland, C. C., Smith, W. K., and Todd-Brown, K.: Future productivity and  
1235 carbon storage limited by terrestrial nutrient availability, Nature Geoscience, 8, 441, 2015b.

1236 Wieder, W. R., Lawrence, D. M., Fisher, R. A., Bonan, G. B., Cheng, S. J., Goodale, C. L.,  
1237 Grandy, A. S., Koven, C. D., Lombardozzi, D. L., and Oleson, K. W.: Beyond static  
1238 benchmarking: Using experimental manipulations to evaluate land model assumptions, Global  
1239 Biogeochemical Cycles, 33, 1289-1309, 2019.

1240 Wright, S. J., Turner, B. L., Yavitt, J. B., Harms, K. E., Kaspari, M., Tanner, E. V., Bujan, J.,  
1241 Griffin, E. A., Mayor, J. R., and Pasquini, S. C.: Plant responses to fertilization experiments in  
1242 lowland, species-rich, tropical forests, Ecology, 99, 1129-1138, 2018.

1243 Xu, R. I. and Prentice, I. C.: Terrestrial nitrogen cycle simulation with a dynamic global  
1244 vegetation model, Global Change Biology, 14, 1745-1764, 10.1111/j.1365-2486.2008.01625.x,  
1245 2008.

1246 Yang, X. and Post, W.: Phosphorus transformations as a function of pedogenesis: a synthesis of  
1247 soil phosphorus data using Hedley fractionation method, Biogeosciences, 8, 2907-2916, 2011.

1248 Yang, X., Post, W., Thornton, P., and Jain, A.: The distribution of soil phosphorus for global  
1249 biogeochemical modeling, Biogeosciences, 10, 2525-2537, 2013.

1250 Yang, X., Thornton, P., Ricciuto, D., and Post, W.: The role of phosphorus dynamics in tropical  
1251 forests—a modeling study using CLM-CNP, Biogeosciences, 11, 1667-1681, 2014.

1252 Yang, X., Thornton, P. E., Ricciuto, D. M., and Hoffman, F. M.: Phosphorus feedbacks  
1253 constraining tropical ecosystem responses to changes in atmospheric CO<sub>2</sub> and climate,  
1254 Geophysical Research Letters, 43, 7205-7214, 10.1002/2016GL069241, 2016.

1255 Yang, X., Wittig, V., Jain, A., and Post, W.: Integration of nitrogen cycle dynamics into the  
1256 Integrated Science Assessment Model for the study of terrestrial ecosystem responses to global  
1257 change, Global Biogeochemical Cycles, 23, 2009.

1258 Yang, X., Ricciuto, D. M., Thornton, P. E., Shi, X., Xu, M., Hoffman, F., and Norby, R. J.: The  
1259 effects of phosphorus cycle dynamics on carbon sources and sinks in the Amazon region: a  
1260 modeling study using ELM v1, Journal of Geophysical Research: Biogeosciences, 2019.

1261 Zaehle, S., Friend, A., Friedlingstein, P., Dentener, F., Peylin, P., and Schulz, M.: Carbon and  
1262 nitrogen cycle dynamics in the O-CN land surface model: 2. Role of the nitrogen cycle in the  
1263 historical terrestrial carbon balance, Global Biogeochemical Cycles, 24, 2010.

1264 Zhang, Q., Wang, Y.-P., Matear, R., Pitman, A., and Dai, Y.: Nitrogen and phosphorous  
1265 limitations significantly reduce future allowable CO<sub>2</sub> emissions, Geophysical Research Letters,  
1266 41, 632-637, 2014.

1267 Zhu, Q., Riley, W. J., Tang, J., Collier, N., Hoffman, F. M., Yang, X., and Bisht, G.:  
1268 Representing nitrogen, phosphorus, and carbon interactions in the E3SM land model:  
1269 Development and global benchmarking, Journal of Advances in Modeling Earth Systems, 11,  
1270 2238-2258, 2019.

1271

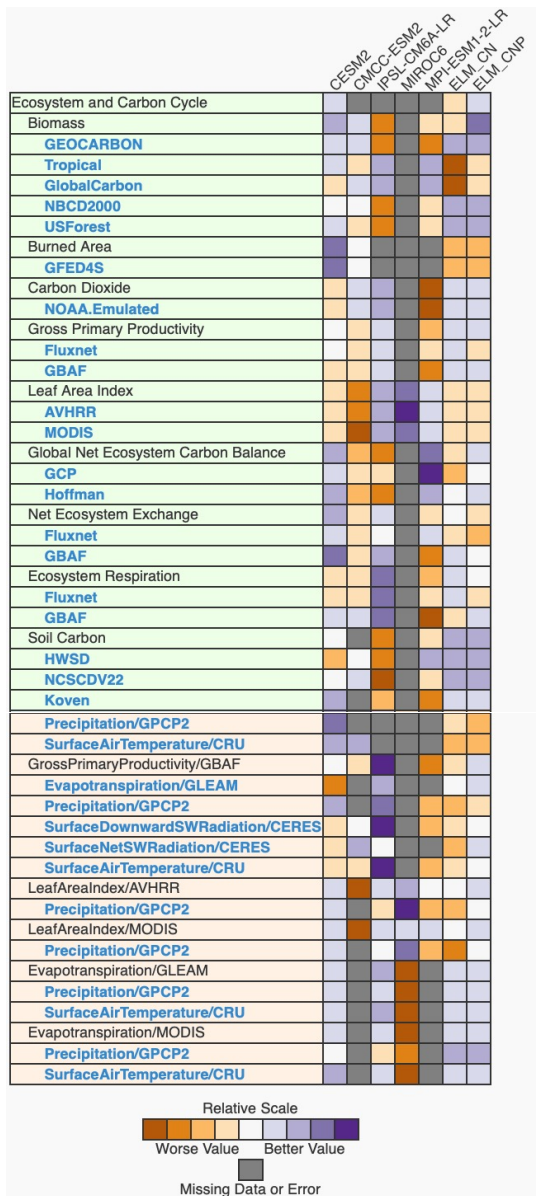
1272

1273

1274

1275  
1276  
1277  
1278  
1279  
1280  
1281  
1282  
1283  
1284  
1285  
1286  
1287

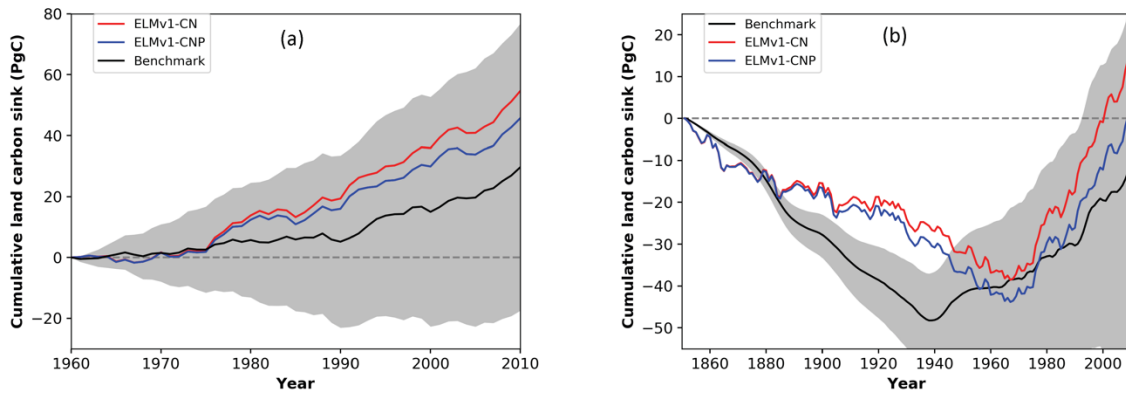




1288

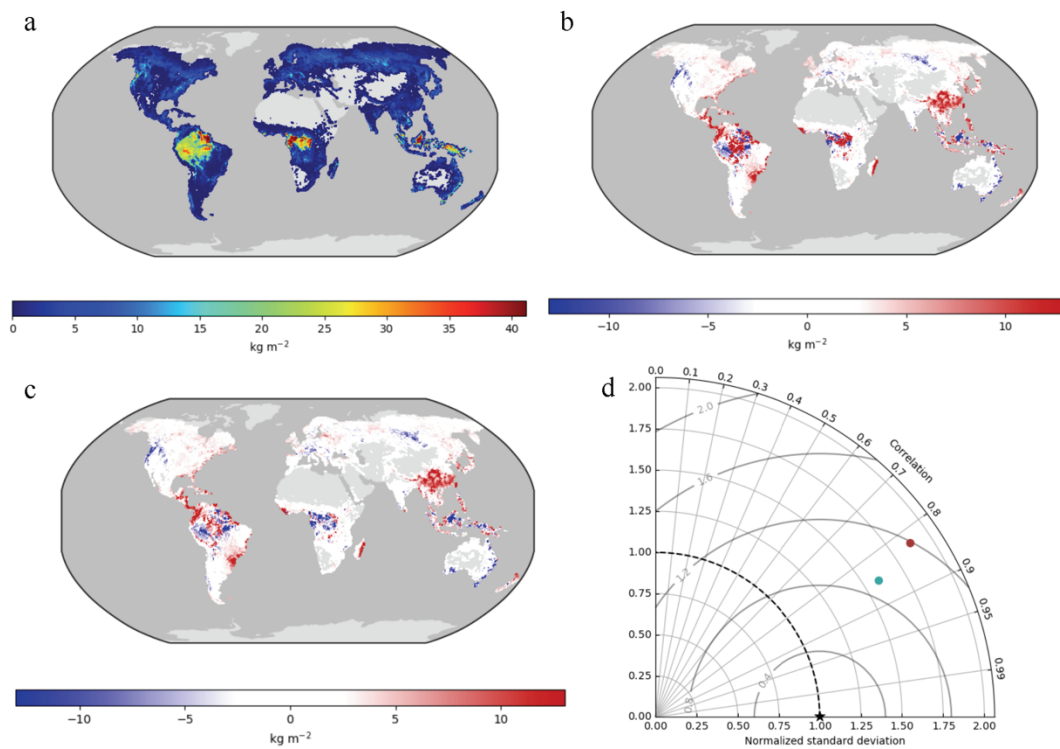
1289 Figure 1: ILAMB carbon cycle scores for ELMv1-CNP and ELM-CN and a few land models in  
 1290 CMIP6. Shown here is the relative score, indicating the performance of each model relative to  
 1291 other models. References for benchmarking data for each variable are provided in Table S4. The  
 1292 datasets that are in green boxes are either carbon pools or fluxes while the datasets in orange  
 1293 boxes are relationships between carbon pools/fluxes and environmental variables such as  
 1294 precipitation or temperature. Outputs for other land models are from the LS3MIP offline  
 1295 simulations archive in CMIP6. These simulations were performed using the same resolution and  
 1296 forcing data as this study. CLM4.5 is the land model in CMCC-ESM2. CLM5 is the land model for

1297 CESM2. OCHIDEE is the land model for IPSL. JSBACH is the land model for MPI-ESM1.2. VISIT is  
1298 the land model for MIROC6.



1299  
1300 Figure 2: ELMv1-CNP and ELMv1-CN simulated global land carbon accumulation for the time  
1301 period (a) 1960-2010 and (b) and 1850-2010. Benchmark data (black lines with uncertainty  
1302 estimate in grey) are from (a) Global carbon project (Le Quere et al., 2016) and (b) Hoffman et  
1303 al. (2014).

1304  
1305  
1306



1307

1308

1309

1310 Figure 3: Global pattern of simulated biomass: (a) benchmark data, (b) ELMv1-CN bias (c)

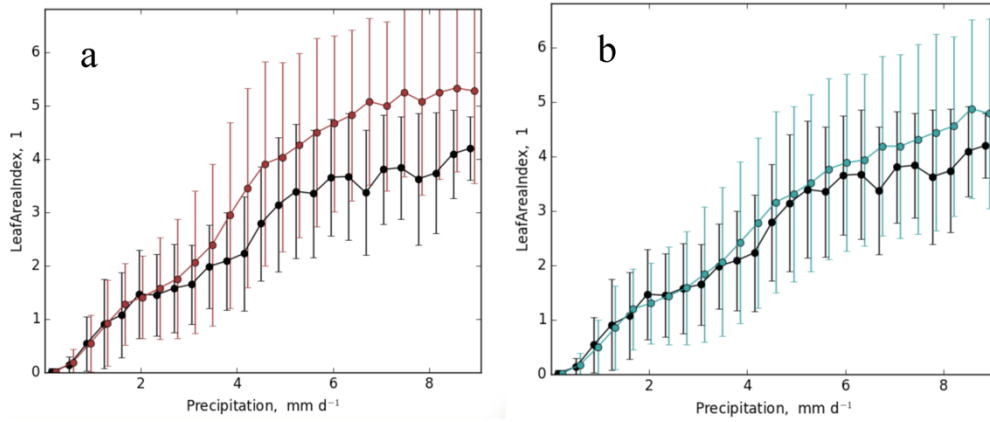
1311 ELMv1-CNP bias and (d) spatial Taylor diagram for model-benchmark comparison (red dot is for

1312 ELMv1-CN and blue dot is for ELMv1-CNP). Benchmark data here is from the GEOCARBON

1313 product (Saatchi et al.,2011).

1314

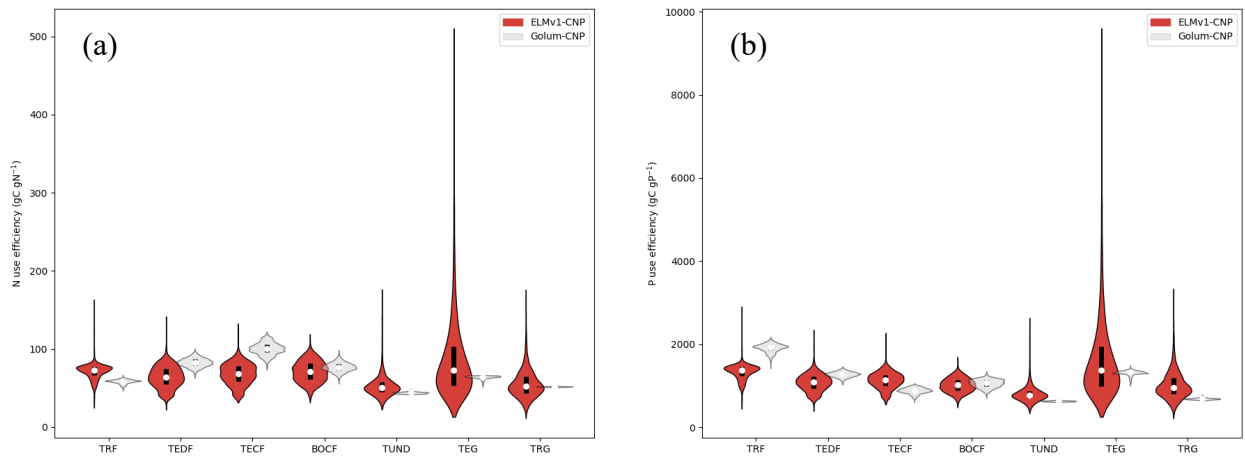
1315



1316  
1317

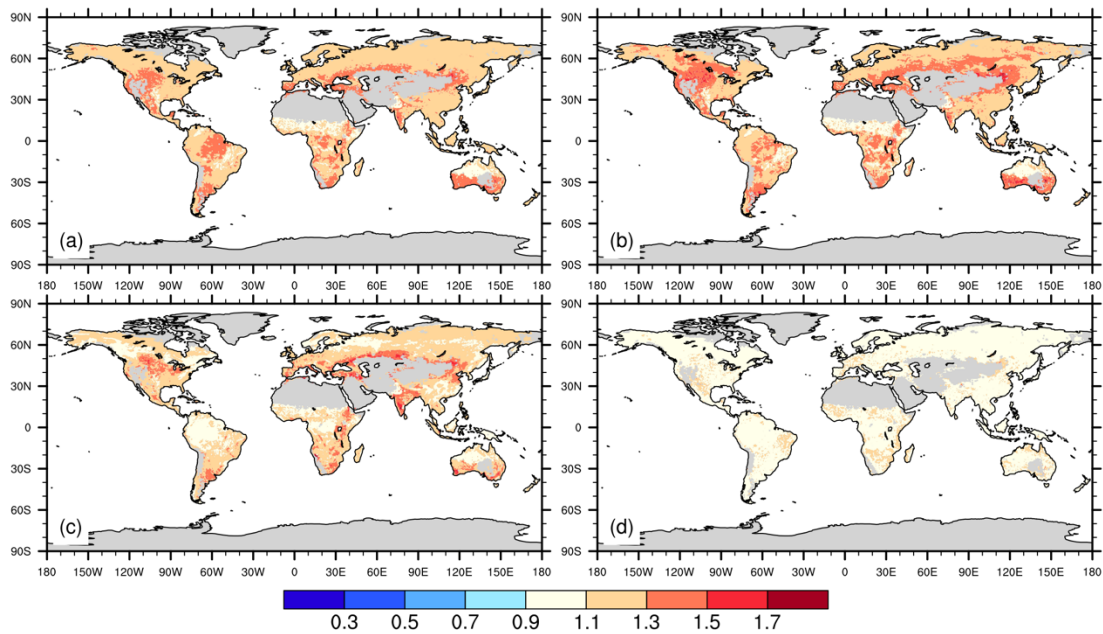
1318 Figure 4: ILAMB relationship plot between LAI and climatological annual precipitation and (a)  
1319 ELMv1-CN (b) ELMv1-CNP. Black line is the observationally derived relationship. Error bars  
1320 indicate one standard derivation of LAI for all grid cells within the precipitation bin. Observed  
1321 LAI is from MODIS LAI product.

1322  
1323  
1324  
1325  
1326  
1327  
1328  
1329



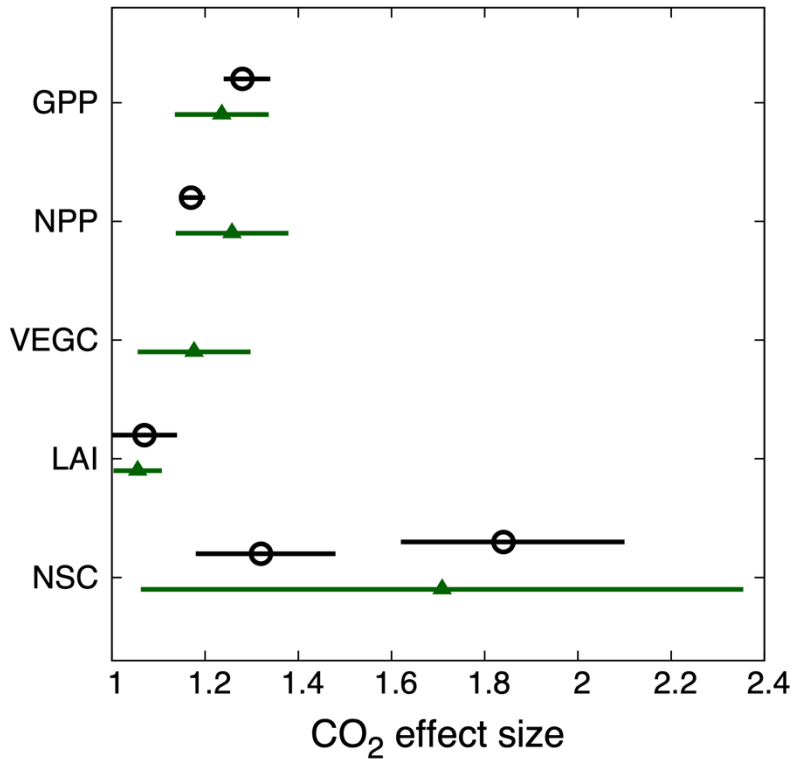
1330  
 1331  
 1332  
 1333  
 1334  
 1335  
 1336  
 1337  
 1338  
 1339  
 1340

Figure 5: Violin plots of (a) nitrogen use efficiency (NUE) and (b) phosphorus use efficiency (PUE) from ELMv1-CNP and GOLUM-CNP for seven biomes: tropical rainforest (TRF), temperate deciduous forest (TEDF), temperate coniferous forest (TECF), boreal coniferous forest (BOCF), temperate grassland (TEG) and tropical grassland (TRG). Plots show the medians of all grid cells in each biome (open circles) and the probability density distribution (balloons).



1341  
 1342  
 1343  
 1344  
 1345  
 1346  
 1347

Figure 6: Spatial distribution of the effect size of CO<sub>2</sub> enrichment on (a) GPP (b) NPP (c) Vegetation carbon (d) LAI. Effect sizes were calculated for each grid cell as the mean annual values of GPP, NPP, vegetation carbon and LAI from CO<sub>2</sub> enrichment simulation divided those from the control simulations between 2001-2010.

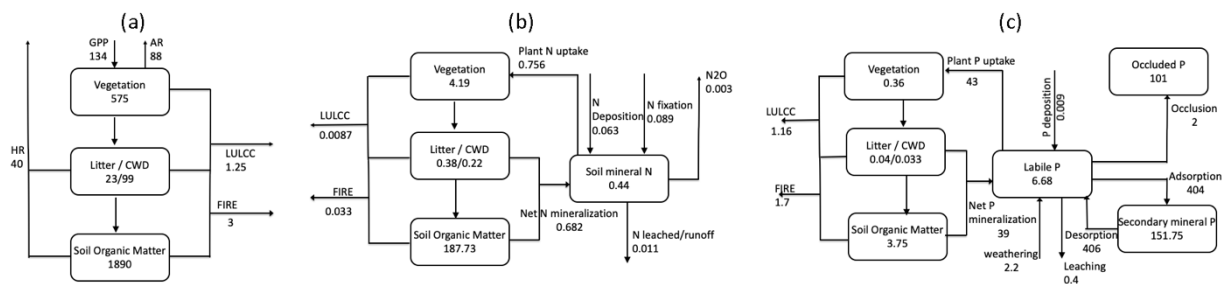


1348

1349 Figure 7: Observed (open circles) and simulated (green triangles) effect size of CO<sub>2</sub> enrichment  
 1350 on GPP, NPP, LAI, vegetation carbon and non-structural carbon. Observations show the mean  
 1351 ( $\pm 95\%$  confidence interval; Ainsworth and Long, 2005). There are two observations of NSC  
 1352 shown here, one is for sugar with a mean value of 1.3 and the other is for starch with a mean  
 1353 value of 1.8, while model conceptualization of NSC includes both sugar and starch. Simulated  
 1354 responses show the global mean effect sizes ( $\pm$  stand derivation; calculated to provide an  
 1355 estimate of spatial variation).

1356

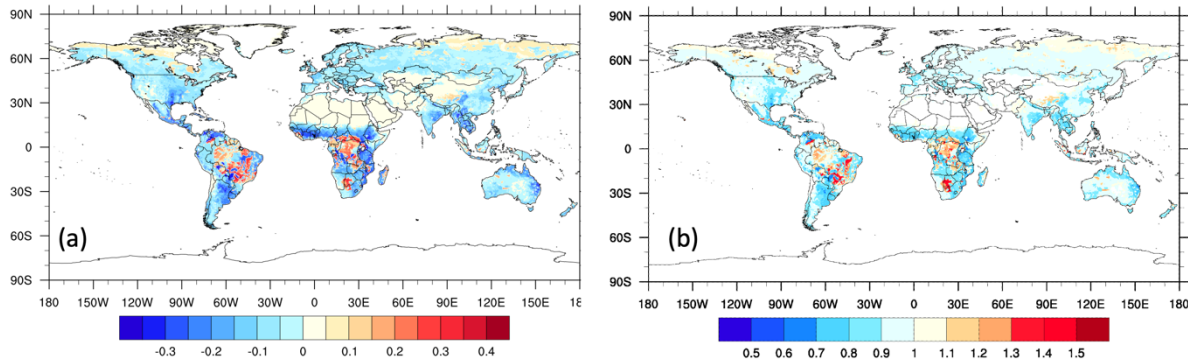
1357



1358  
 1359  
 1360  
 1361  
 1362  
 1363  
 1364  
 1365  
 1366  
 1367  
 1368  
 1369  
 1370  
 1371  
 1372  
 1373  
 1374  
 1375

Figure 8: (left) terrestrial C cycle, (middle) N cycle, and (right) P cycle as simulated by ELMv1-CNP, shown here are mean values between 2001-2010. Vegetation and soil C, N and P pools are in units of Pg C, Pg N and Pg P, respectively. C and N fluxes are given in Pg C yr<sup>-1</sup> and Pg N yr<sup>-1</sup>, and P fluxes are given in Tg P yr<sup>-1</sup>. AR stands for autotrophic respiration and HR stands for heterotrophic respiration.





1376

1377 Figure 9: (a) Spatial variation of the extent of nutrient limitation on plant growth. Regions with  
 1378 a negative value are more limited by N, while regions with a positive value are more limited by  
 1379 P. Larger absolute values are associated with stronger limitation. Values plotted are the  
 1380 proportion by which plant growth is reduced due to N limitation or P limitation:  $1-f_P$  when  $f_P$   
 1381  $< f_N$  and  $f_N-1$  when  $f_N < f_P$ , where  $f_P$  is the limitation factor on plant growth considering P  
 1382 supply and demand, while  $f_N$  is the limitation factor on plant growth considering N supply and  
 1383 demand (Yang *et al.*, 2014). (b) Spatial variation of the ratios between P limitation and N  
 1384 limitation indicating the degree of co-limitation. Values plotted are the ratios between  $f_N$  and  
 1385  $f_P$ :  $f_N/f_P$ . Regions with values less than 1 indicate more N limitation and regions with values  
 1386 greater than 1 are more limited by P. Values close to 1 indicate NP co-limitation. Definition of  
 1387 colimitation is subjective here, but difference of 10% or less between the values for  $f_N$  and  $f_P$   
 1388 would lead to a range of about 0.9 to 1.1 in the plotted ratio.

1389

1390

1391

1392

1393

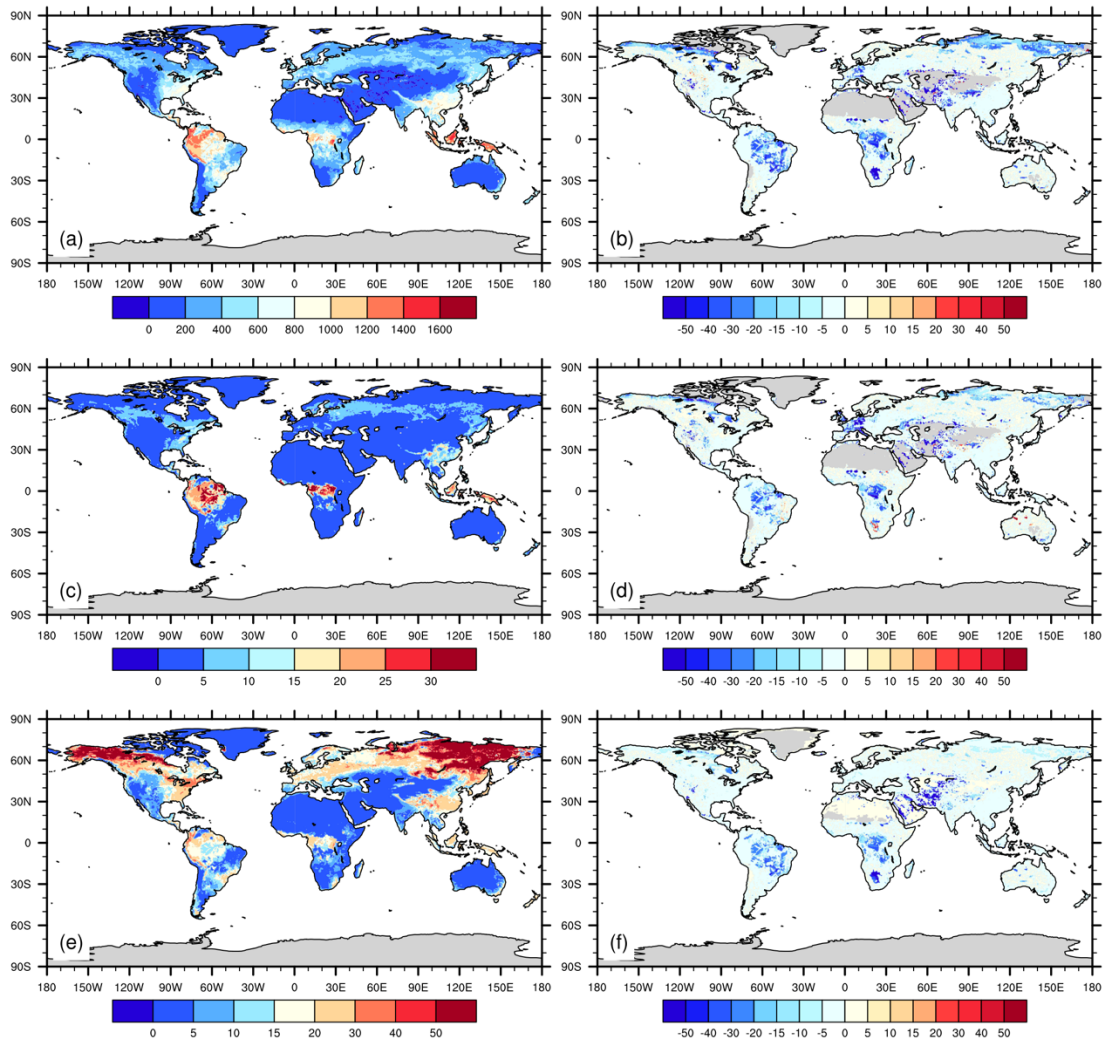
1394

1395

1396

1397

1398



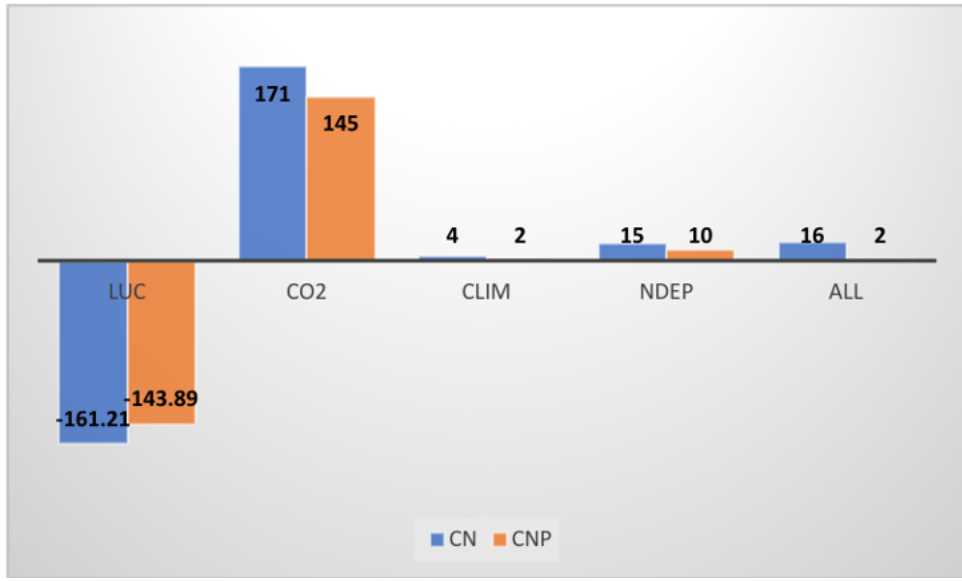
1400

1401

1402 Fig. 10: Average estimates of (a) net primary productivity ( $\text{g C m}^{-2} \text{ yr}^{-1}$ ) (c) vegetation carbon ( $\text{kg C m}^{-2}$ ) and (e) soil organic carbon ( $\text{kg C m}^{-2}$ ) for the years 2001-2010 and the effects of  
 1403  $\text{C m}^{-2}$ ) and (e) soil organic carbon ( $\text{kg C m}^{-2}$ ) for the years 2001-2010 and the effects of  
 1404 phosphorus dynamics (expressed as percentage deviation between CNP and CN configurations,  
 1405 unitless) on (b) net primary productivity (d) vegetation carbon (f) soil carbon as estimated by  
 1406 ELMv1.

1407

1408



1409

1410 Fig. 11: Cumulative global carbon storage (Pg C) from 1850 to 2010 from ELMv1-CN and ELMv1-  
 1411 CNP simulations with changes in land use and land cover change (LUC), atmospheric CO<sub>2</sub> (CO<sub>2</sub>),  
 1412 climate (CLIM), N deposition (NDEP), and all factor combined (ALL). These are calculated as the  
 1413 accumulation of NEE between 1850 and 2010 for the historical transient model simulations  
 1414 listed in Table 1.

1415

1416

1417

1418

1419

1420

1421

1422

1423

1424

1425

1426

1427

1428

1429  
1430  
1431

Table 1: Summary of model simulations

Experiment	P coupling	CO <sub>2</sub> forcing	LULCC	Climate forcing	N depos
Ctrl_CN	off	1850	1850	steady state <sup>a</sup>	1850
Ctrl_CNP	on	1850	1850	steady state <sup>a</sup>	1850
Hist_CN_CO <sub>2</sub>	off	transient	1850	steady state <sup>a</sup>	1850
Hist CNP CO <sub>2</sub>	on	transient	1850	steady state <sup>a</sup>	1850
Hist_CN_LUC	off	1850	transient	steady state <sup>a</sup>	1850
Hist CNP LUC	on	1850	transient	steady state <sup>a</sup>	1850
Hist CN climate	off	1850	1850	transient <sup>b</sup>	1850
Hist_CNP_ climate	on	1850	1850	transient <sup>b</sup>	1850
Hist CN NDep	off	1850	1850	steady state <sup>a</sup>	transient
Hist_CNP_Ndep	on	1850	1850	steady state <sup>a</sup>	transient
Hist CN all	off	Transient	A d	transient <sup>b</sup>	transient
Hist CNP all	on	transient	transient	transient <sup>b</sup>	transient
FACE_CO <sub>2</sub>	on	+200ppm (1991-2010)	transient	transient <sup>b</sup>	transient

1432 a Cycling of 20-year time series of GSWP3 reanalysis product (1901-1920)

1433 b Historical time series of GSWP3 reanalysis product (1901-2010)

1434  
1435

1436

1437

1438

1439

1440

1441

1442

1443

1444

1445

1446

1447

1448

1449 Table 2: Comparison of ELMv1-CNP Simulated Mean Global Stocks and Fluxes of C, N and P  
 1450 between 2001 and 2010 to Observation-based Estimates

	ELMv1-CNP	Observation-based Estimates		
			Source	Methodology
GPP (Pg C yr <sup>-1</sup> )	134.15	123±8	Beer et al., 2010	Using eddy covariance flux data and various diagnostic models
		150-175	Welp et al., 2011	Based on oxygen isotopes of atmospheric CO <sub>2</sub>
		119±6	Jung et al., 2011	upscaled FLUXNET observations to the global scale using the machine learning technique, model tree ensembles (MTE).
		121.60 - 129.42	Zhang et al., 2017	Light use efficiency theory, MODIS satellite data and climate data
		140	Joiner et al., 2018	Satellite Data-Driven Models and Eddy Covariance Flux Data
NPP (Pg C yr <sup>-1</sup> )	46.09	55±11	Turner et al., 2006	MODIS products
		33-49	Smith et al., 2016	MODIS NPP algorithm driven by long-term Global Inventory Modeling and Mapping Studies (GIMMS) FPAR and LAI data
Vegetation C (Pg C)	575.45	550±100	Houghton, 2003	Literature synthesis
		560±94	Defries et al., 1999	
Soil carbon (Pg C)	1890.78	1750±250	Houghton, 2003	Literature synthesis
		2344	Jobbagy and Jackson, 2000	based on >2700 soil profiles in three global databases supplemented with data for climate, vegetation, and land use.
		3000	Kochy et al., 2015	Based on the Harmonized World Soil Database(HWSD), but with more detailed estimates for permafrost and tropical wetland soil carbon
		2376–2456	Batjes, 2014	Top 2m. Based on 4353 soil profiles distributed globally and the FAO Soil Map of the World.
Top 1m soil carbon (Pg C)	1134.41	1462-1548	Batjes, 2014	Based on 4353 soil profiles distributed globally and the FAO Soil Map of the World.
		1325	Kochy et al., 2015	Based on the Harmonized World Soil Database(HWSD), but with more detailed estimates for permafrost and tropical wetland soil carbon
		1502	Jobbagy and Jackson, 2000	based on >2700 soil profiles in three global databases supplemented with

				data for climate, vegetation, and land use.
Soil organic N (Pg N)	188.79	95	Post et al. 1985	Based on 3100 soil profiles and a global map of Holdridge life zones
		133-140	Batjes et al., 2014	Top 1m. Based on 4353 soil profiles distributed globally and the FAO Soil Map of the World
N fixation (Tg N yr <sup>-1</sup> )	89	40-100	Vitousek et al., 2013	Estimates for Pre-industrial. Combining information on N fluxes with <sup>15</sup> N relative abundance data for terrestrial ecosystems
		52-130	Davies-Barnard and Friedlingstein (2020)	Based on a comprehensive meta-analysis of field measurements
N uptake (Tg N yr <sup>-1</sup> )	760	570	Wang et al., 2018	Data-driven estimates. Observations include observed stoichiometric ratios, N and P external input fluxes, and the fraction of gaseous losses of N to total (gaseous and leaching) losses of N from a global data set of <sup>15</sup> N measurements in soils
N Leaching (Tg N yr <sup>-1</sup> )	12	38	Wang et al., 2018	Data-driven estimates. See above
		28	Mayorga et al., 2010	based on a mass-balance approach for the land surface (watershed) and river system for year 2000
P uptake (Tg P yr <sup>-1</sup> )	43	26	Wang et al., 2018	Data-driven estimates. See above
P leaching (Tg P yr <sup>-1</sup> )	0.46	2.6	Wang et al., 2018	Data-driven estimates. See above
P occlusion (Tg P yr <sup>-1</sup> )	1.85	1.3	Wang et al., 2018	Data-driven estimates. See above

1451  
1452  
1453  
1454  
1455  
1456  
1457  
1458  
1459  
1460  
1461  
1462  
1463  
1464  
1465